HHS Public Access

Author manuscript

Br J Pharmacol. Author manuscript; available in PMC 2023 August 01.

Published in final edited form as:

Br J Pharmacol. 2023 August ; 180(15): 1930–1948. doi:10.1111/bph.16058.

A novel sorbicillinoid compound as a potent anti-inflammation agent through inducing NLRP3 protein degradation

Fangfang Wang[1,2], **Meng Zhang**[1], **Meng Yuan**[1], **Zixuan Xia**[1], **Fengge Yang**[1], **Sihao Zhang**[1], **Tengyu Lin**[3], **Lianxiang Luo**[3,4], **Jinshan Tang**[1], **Youwei Zhang**[2]

[1]Guangdong Province Key Laboratory of Pharmacodynamic Constituents of Traditional Chinese Medicine and New Drug Research, International Cooperative Laboratory of Traditional Chinese Medicine Modernization and Innovative Drug Development of Ministry of Education (MOE) of China, Institute of Traditional Chinese Medicine and Natural Products, College of Pharmacy, Jinan University, Guangzhou, China

[2]Department of Pharmacology, Case Comprehensive Cancer Center, Case Western Reserve University School of Medicine, Cleveland, Ohio, USA

[3]The Marine Biomedical Research Institute, Guangdong Medical University, Zhanjiang, China

[4]The Marine Biomedical Research Institute of Guangdong Zhanjiang, Zhanjiang, China

Abstract

Background and Purpose: Chronic inflammation is pathogenic and contributes to human diseases, causing a significant threat to public health. The NLR family pyrin domain-containing protein 3 (NLRP3) is the best-characterized factor regulating inflammation. Therefore, targeting NLRP3 has the potential to treat inflammatory diseases and improve human health.

Correspondence: Lianxiang Luo, The Marine Biomedical Research Institute of Guangdong Zhanjiang, Zhanjiang, China. luolianxiang321@gdmu.edu.cn, Jinshan Tang, Guangdong Province Key Laboratory of Pharmacodynamic Constituents of Traditional Chinese Medicine and New Drug Research, International Cooperative Laboratory of Traditional Chinese Medicine Modernization and Innovative Drug Development of Ministry of Education (MOE) of China, Institute of Traditional Chinese Medicine and Natural Products, College of Pharmacy, Jinan University, Guangzhou, China. jstang0615@jnu.edu.cn, Youwei Zhang, Department of Pharmacology, Case Comprehensive Cancer Center, Case Western Reserve University School of Medicine, Cleveland, OH, USA. yxz169@case.edu.

Fangfang Wang, Meng Zhang and Meng Yuan contributed equally to this work.

AUTHOR CONTRIBUTIONS

Fangfang Wang: methodology, data collection and analysis, and manuscript writing. **Meng Zhang:** synthesis of JNUTS013 and analogues. **Meng Yuan, Zixuan Xia** and **Sihao Zhang:** data collection and analysis during revision. **Fengge Yang:** assistance in acute liver injury animal studies. **Tengyu Ling:** assistance in DSS-induced ulcerative colitis animal experiment. **Lianxiang Luo:** conceptual contribution to the *Nlrp3* knockout mice experiment and data collection. **Jinshan Tang** and **Youwei Zhang:** conceptualization, data analysis and manuscript writing. All authors have read the content of the manuscript and proved its publication.

CONFLICT OF INTEREST STATEMENT

The authors declare that they have no competing interests.

DECLARATION OF TRANSPARENCY AND SCIENTIFIC RIGOUR

This Declaration acknowledges that this paper adheres to the principles for transparent reporting and scientific rigour of preclinical research as stated in the *British Journal of Pharmacology* guidelines for Design and Analysis, Immunoblotting and Immunochemistry and Animal Experimentation, and as recommended by funding agencies, publishers and other organizations engaged with supporting research.

SUPPORTING INFORMATION

Additional supporting information can be found online in the Supporting Information section at the end of this article

Experimental Approach: **Lipopolysaccharide** was used to induce inflammation in cell cultures. Lipopolysaccharide/D-galactosamine and dextran sulfate sodium salt were used to induce acute liver inflammation and ulcerative colitis respectively in C57BL/6J mice. Western blotting, immunofluorescence, immunoprecipitation, quantitative PCR and enzyme-linked immunosorbent assay (ELISA) were used to evaluate the activation of the inflammatory response in cell cultures and in mice.

Key Results: JNUTS013, a novel sorbicillinoid compound recently synthesized by us, significantly inhibited inflammation both in cell cultures and in mouse models. Mechanistically, JNUTS013 induced proteasome-dependent degradation of NLRP3. Hence, it suppressed the formation of the NLRP3 inflammasome and the production of downstream inflammatory cytokines and chemokines. The inhibitory effect of JNUTS013 on NLRP3 protein expression was confirmed in mice. Importantly, JNUTS013 failed to ameliorate bowel inflammation in *Nlrp3*$^{-/-}$ knockout mice, supporting NLRP3 as the biological target by which JNUTS013 inhibits inflammation. Further studies revealed critical chemical moieties of JNUTS013 required for inducing NLRP3 degradation.

Conclusion and Implications: This study identifies a novel compound JNUTS013 that inhibits inflammation through inducing NLRP3 protein degradation *in vitro* and *in vivo*, which not only supports the development of JNUTS013 as an anti-inflammation agent but also creates a new way for treatment of inflammation by chemically inducing NLRP3 degradation.

Keywords

acute liver injury; anti-inflammatory agent; inflammation; JNUTS013; NLRP3; protein degradation; ulcerative colitis

1 | INTRODUCTION

Classical inflammation is an ancient innate immunity towards foreign pathogens and cellular by-products known as pathogen-associated molecular patterns (**PAMP**s) and damage-associated molecular patterns (**DAMP**s), respectively (Liu et al., 2021; Shalapour & Karin, 2015). Inflammation activation is characterized by the formation of cytosolic multimeric protein complexes, the so-called inflammasomes (Broz & Dixit, 2016). Inflammasomes generally consist of either a nucleotide-binding domain **leucine-rich repeat** (**NLR**)- or a pyrin and **HIN domain (PYHIN)**-type receptor as the sensor and the adaptor protein, apoptosis-associated speck-like (ASC; PYCARD) to form four sub-types: **NLRP1, NLRP3, NLRC4** and **absent in melanoma 2 (AIM2)** (Rathinam et al., 2012). The NLRP3 inflammasome is most widely studied and composed of NLRP3, ASC and pro-**caspase-1**, whose assembly may take place at the microtubule-organizing centre with the aid of **histone deacetylase 6** (Magupalli et al., 2020).

Activation of the NLRP3 inflammasome involves two steps, priming and activating (Kelley et al., 2019). In the priming stage, **PAMPs** or DAMPs bind to **toll-like receptors (TLRs)** to activate the nuclear factor-κB (NF-κB) pathway to induce the transcription of *NLRP3*, **pro-IL-1β gene, IL1B** and **pro-IL-18 gene, IL18** and so on (Walsh et al., 2013; Wicherska-Pawlowska et al., 2021), promoting the assembly of the NLRP3-ASC-pro-

caspase-1 inflammasome. In the activating stage, cells are stimulated with agonists such as **ATP** to induce autocleavage of pro-caspase-1, leading to the production of mature caspase-1 (Dick et al., 2016; Lu et al., 2014), which then will cleave molecules such as pro–IL-1β into its mature form to promote inflammation (Brough et al., 2017; Swanson et al., 2019). Well-controlled activation of NLRP3 is protective against pathogen invasion or endogenous stress. However, pathological activation of NLRP3 or inflammation is associated with various chronic diseases such as rheumatoid arthritis and osteoarthritis (Guo et al., 2018; Jin & Fu, 2019; McAllister et al., 2018; Pirzada et al., 2020), atherosclerosis (Jin & Fu, 2019), multiple sclerosis (Olcum et al., 2020), type 2 diabetes (Jin & Fu, 2019), neurodegeneration (Halle et al., 2008; Heneka et al., 2013; Wang, Chi, et al., 2020) and cancer (Mayca Pozo et al., 2021; Zahid et al., 2019).

Given its importance in inflammation, NLRP3 has remained a central target in the design of strategies that treat inflammatory diseases and many small molecule inhibitors have been developed (Zahid et al., 2019). For example, **MCC950**, a widely studied NLRP3 inhibitor and also known as CRID3 or CP-456773 (Coll et al., 2015; Laliberte et al., 2003), binds the NACHT region of NLRP3 to keep the protein in the inactive state (Dekker et al., 2021; Hochheiser et al., 2022; Ohto et al., 2022). However, most, if not all known inhibitors target the NLRP3-dependent inflammation signalling and none have been reported to specifically induce NLRP3 degradation.

Previously, we isolated sorbicillinoid compounds from marine fungi that showed promising anti-inflammatory activities (Ding et al., 2021). We further synthesized novel analogues and discovered one (JNUTS013; see Figure 1a for structure) with strong anti-inflammation potential (Zhang, Wang, et al., 2022). Here, we comprehensively assessed the anti-inflammation effect of JNUTS013 in both macrophage-lineage mouse and human cell lines and in mouse models. We investigated the underlying mechanism and identified NLRP3 as the cellular target by which JNUTS013 suppresses inflammation.

2 | METHODS

2.1 | Cell culture and treatment

RAW264.7 (Cat#400319/p462, RRID:CVCL_0493) and THP-1 (Cat#0356, RRID:CVCL_0006) cells were obtained from American Type Culture Collection (ATCC, Manassas, VA, USA). BV2 (Cat#ABC-TC212S, RRID:CVCL_0182) was obtained from Accegen Biotechnology (Fairfield, New Jersey, USA). RAW264.7 and BV2 cells were grown in Dulbecco's modified Eagle's medium (DMEM) (Cat#C11995500CP, Gibco/Thermo Fisher, Carlsbad, USA) with 10% (v/v) FBS (Cat#11F364, ExCell Bio, China). Human THP-1 cells were cultured in RPMI 1640 medium (Cat#C11875500BT, Gibco, Carlsbad, USA) with 10% (v/v) FBS, 0.05 mM β-mercaptoethanol and 1 mM sodium pyruvate. To differentiate THP-1 cells into macrophages, PMA (200 nM) was added to the culture media for 3 days. All cells were cultured in a humidified atmosphere with 5% CO_2 at 37°C.

2.2 | Measurement of cell viability

3-(4,5-Dimethylthiazol-2-yl)-2,5-diphenyltetrazolium bromide (MTT) assay was used to determine cell viability in the presence or absence of compound treatment as previously reported with modifications (Geng et al., 2020). Briefly, RAW264.7, BV2 or THP-1 cells were seeded in a 96-well plate (1.0×10^4 cells per well) and treated with **lipopolysaccharide** (**LPS**; 0.5 $\mu g ml^{-1}$), JNUTS013 (various concentration) or the combination for different time. Then 20 μl MTT (5 $mg ml^{-1}$) were added into each well and cultured for an additional 4 h. Subsequently, DMSO (150 μl per well) was added to extract the purple formazan dye from cells. Absorbance was determined at 570 nm using a microplate reader (BioTek, synergy HT, USA).

2.3 | Nitric oxide (NO) measurement

NO release in the cell culture media was measured by the Griess reaction kit (Cat# S0021S, Beyotime Biotech, Shanghai, China). RAW264.7 and BV2 cells were counted and seeded into a 96-well plate (1.0×10^4 cells per well) and cultured overnight. After treated with LPS (0.5 $\mu g ml^{-1}$), different concentrations of JNUTS013 or other agents, or this combination for different time, a 50 μl supernatant were taken out and added into a new 96-well plate and added liquid A and liquid B sequentially based on the manufacturer's instructions. After incubating for 10 min at room temperature, the NO content was measured at 540 nm using a microplate reader (BioTek, synergy HT, USA).

2.4 | Western blotting

Western blotting was performed as previously described with modifications (Tian et al., 2020; Wang et al., 2022) and the immuno-related procedures used comply with the recommendations made by the *British Journal of Pharmacology* (Alexander et al., 2018). In brief, cells (2.0×10^6 cells per well) were seeded into 6-well plates and cultured at 37°C overnight. After treated with LPS (0.5 $\mu g ml^{-1}$) with or without different concentrations of JNUTS013 or other agents, cells were collected and washed with cold PBS twice, lysed in RIPA buffer (Cat#P1003B, Beyotime Biotech, Shanghai, China) containing protease inhibitors (Cat#ST506 and SG2004, Beyotime Biotech, Shanghai, China), sonicated and centrifuged to harvest total proteins. The BCA protein assay kit (Cat#23225, Thermo/Pierce, MA, USA) was used to measure the protein concentration. Equal amount of protein samples (40–70 μg applied to each lane) was separated by sodium dodecyl sulfate polyacrylamide gel electrophoresis (SDS-PAGE) (6%–10%) and transferred to polyvinylidene fluoride (PVDF) membrane (Cat#IPVH00010, Millipore, Billerica, MA, USA). The PVDF membranes were blocked with 5% skim milk for 1 h at room temperature, washed 8 min three times in tris buffered saline with tween (TBST) and incubated with primary antibodies (diluted in TBST buffer at 1:1000) specific for NLRP3 (Cell Signaling Technology, clone D4D8T, Cat#15101, rabbit monoclonal, RRID:AB_2722591), ASC (Santa Cruz Biotechnology, clone B-3, Cat#SC-514414, mouse monoclonal, RRID:AB_1121554), **iNOS** (Cell Signaling Technology, clone D6B6S, Cat#13120, rabbit monoclonal, RRID:AB_2687529), p-IkBα (Cell Signaling Technology, S32/36, clone 5A5, Cat#9246, mouse monoclonal, RRID:AB_2267145), Chk1 (Santa Cruz Biotechnology, clone DCS-310, Cat#SC-56291, mouse monoclonal, RRID:AB_1121554),

IL-1β (R&D systems, Cat#AF-401-NA, goat polyclonal, RRID:AB_416684), ubiquitin like with PHD and ring finger domains 1 (UHRF1; Santa Cruz Biotechnology, clone H8, Cat#SC-373750, mouse monoclonal, RRID:AB_10947236), p-mTOR (Cell Signaling Technology, S2448, clone D9C2, Cat#5536, rabbit monoclonal, RRID:AB_10691552) and β-Actin (Bioworld Technology, clone 4D3, Cat#BS6007M, mouse monoclonal, RRID:AB_2904238) for 4 h at room temperature or overnight at 4°C. The membranes were washed with TBST for 8 min five times, incubated with HRP-conjugated goat anti-rabbit (Thermo/Pierce, Cat#PI-31460) or anti-mouse (Thermo/Pierce, Cat#PI-31430) secondary antibodies for 1 h at room temperature, washed with TBST five times each for 8 min, reacted with an ECL solution (Cat#FD8020, Fdbio science) and detected by the Tanon imaging system (BioTanon, Shanghai, China). Quantitation of the band intensity was analysed by the ImageJ software (RRID:SCR_003070).

2.5 | Quantitative polymerase chain reaction (qPCR)

qPCR reactions were performed on a CFX96 Real-Time PCR system (Bio-Rad, Hercules, CA, USA) with Qiagen SYBR Green Master Mix (Cat#208054, Germany Town, MD, USA) as previously described (Wang, Mayca Pozo, et al., 2020) and followed the minimum information for publication of quantitative real-time PCR experiments (minimum information for publication of quantitative real-time PCR; MIQE) guidelines. Briefly, after 12 h treatment with JNUTS013 (10 μM) and/or LPS (0.5 $\mu g ml^{-1}$), total cellular RNA was extracted from RAW264.7 cells using the Qiagen RNeasy plus kit (Cat#74134, Germany Town, MD, USA) and quantified by measuring the absorbance with the nanodrop spectrophotometer (ND 1000, Thermo/Fisher Scientific, Waltham, MA, USA). Twelve micrograms of cDNA was reverse transcribed with the Revert Aid first strand cDNA synthesis kit (Cat#K1622, Thermo Scientific, Franklin, MA, USA). The relative mRNA level of target genes was calculated according to formula $2^{-\Delta\Delta Ct}$ using hypoxanthine-guanine phosphoribosyltransferase gene (*Hprt1*) as the internal control. Amplification programme started with a hot start at 95°C for 30 s, followed by 40 cycles of denaturation at 95°C for 5 s, annealing at 60°C for 15 s and extension at 72°C for 10 s. The melting curve was assessed using a programme of heating at 95°C for 10 s, 65°C for 30 s followed by a gradual increase to 95°C at a 0.5C increment. qPCR primers used in this study are listed in Table 1.

2.6 | Enzyme-linked immunosorbent assay (ELISA)

The levels of IL-1β and **TNF-α** secreted into the culture media were determined by ELISA. Briefly, after 12 h treatment with JNUTS013 (10 μM) and/or LPS (0.5 $\mu g ml^{-1}$), the supernatant was collected and centrifuged at 1000 *g* for 10 min at 4°C. The protein levels of IL-1β and TNF-α in the culture supernatant were detected by mouse-specific ELISA kits (Cat# CME0015 and Cat#CME0004, 4A Biotech CO., Guangdong, China) according to the manufacturer's instructions. Finally, the absorption at 450 nm was detected using a microplate reader (BioTek, synergy HT, USA).

2.7 | Detection of NLRP3 and ASC aggregate formation

BV2 cells were seeded into 100 mm dishes and cultured overnight. Following drug treatment, cell extracts were acquired using the NP-40 lysis buffer (10 mM Hepes, pH 7.5, 5 mM $MgCl_2$, 142 mM KCl, 1 mM EDTA and 0.5% NP-40), centrifugated at 500 *g* for 10 min, collected the pellet and incubated with freshly made 2 mM DSS solution for 30 min at room temperature. The samples were centrifugated at 500 *g* for 10 min at 4°C, discarded the supernatant, dissolved the pellet with 300 μl RIPA lysis buffer containing 0.1% SDS, sonicated and centrifuged at 10,000 *g* for 10 min at 4°C to collect the supernatant, took out 40 μl as the input for protein analysis. The remaining supernatant was incubated with anti-ASC primary antibody at 4°C overnight, added 50 μl pre-washed protein A/G beads and incubated for another 4 h with gentle agitation, centrifugated at 10,000 *g* for 10 s and washed the beads three times with RIPA lysis buffer. The beads were added with 40 μl 2× sample buffer, heated at 95°C for 5 min, cooled down, centrifuged at 10,000 *g* for 5 min, loaded the supernatant to SDS-PAGE gels and detected the level of ASC oligomerization by western blotting.

2.8 | Immunofluorescence

Immunofluorescence staining and confocal imaging were conducted as previously described with modifications (Zhang, Geng, et al., 2022). THP-1 and BV2 cells were both seeded into 6-well plates with glass coverslips at the density of 1×10^6 cell per well. Following treatment, cells on glass coverslips were washed with PBS for 5 min twice, fixed with 4% formaldehyde (pH 7.4) at room temperature for 15 min and washed with PBS for 5 min twice. Subsequently, cells were blocked with PBS containing 5% BSA and 0.2% Triton X100 for 1 h at room temperature, washed with PBS twice, incubated with anti-NLRP3 or anti-ASC primary antibodies (1:500 dilution in PBS) overnight, washed with PBS twice, followed by incubation with Alexafluor-594 (Cat#, A23420, Abbkine Inc., Wuhan, China) or Alexafluor-488 (Cat# A23210, Abbkine Inc., Wuhan, China) conjugated anti-rabbit antibody for 1 h, washed with PBS twice, mounted the glass coverslips onto slides with the Prolong Gold anti-fade solution with DAPI (#P36941, Thermo/Life Technologies). NLRP3 and ASC images were acquired by a confocal microscopy system (LSM 880, Zeiss, Germany) with exposure time maintained the same for each set of experiment. The intensity of immunofluorescence staining of NLRP3 and ASC was analysed by the NIH ImageJ 1.44 software.

2.9 | Measurement of IL-1β content in culture media

To determine the level of IL-1β protein secreted into cultured media by western blotting, we treated RAW264.7 cells with LPS (0.5 $\mu g ml^{-1}$) with or without 10 μM JNUTS013 for 24 h. ATP (5 mM) was added 1 h prior to collecting the supernatant. Five times the volume of cold acetone was added to the supernatant, mixed thoroughly and placed at −80°C overnight to allow protein precipitation. The mixture was centrifuged at 10,000 *g* for 10 min at 4°C, discarded the supernatant and dried the pellet in a fume cupboard to allow acetone to volatilize completely. Added 30 μl RIPA lysis buffer with protease inhibitors to fully dissolve the precipitate, transfer to a new microcentrifuge tube and centrifuge at 10,000 *g* for 10 min at 4°C. Protein concentration in the supernatant was determined by Bradford

Protein Quantification Kit (#20202ES76, Yeasen, Shanghai, China) and analysed by western blotting for IL-1β expression.

2.10 | Detection of NLRP3 protein modification by chemicals *in vitro*

Three 100 mm dishes of BV2 cells were collected and lysed to obtain ~10 mg of total proteins, added 8 μg of anti-NLRP3 antibody, incubated at 4° overnight with gentle rotation, added PBS pre-washed Protein A/G agarose beads (170 μl) and further incubated at 4° for another 3 h, span at 10,000 *g* at 4° for 1 min and discarded the supernatant, washed the beads twice with PBS, added 100 μl PBS to re-suspend the beads, equally divided the bead slurry into five microcentrifuge tubes, added 15 μM JNUTS013 or DSS dissolved in DMSO and added the volume up to 100 μl with PBS. The control group was added the same volume of DMSO. Incubated the beads on ice for 10, 30 or 60 min, span at 10,000 *g* at 4° for 1 min, washed twice with PBS, added 25 μl 2× SDS sample buffer, boiled at 95° for 8 min, cooled down and loaded onto SDS-PAGE, and detected with anti-NLRP3 antibodies.

2.11 | Animals

Wide type (WT) C57BL/6J female mice at the age of 6–8 weeks and weighing 18–22 g were purchased from Beijing Huafukang Bioscience Co., China. Wild type (WT) and *Nlrp3*$^{-/-}$ C57BL/6J female mice were obtained from the Jackson Laboratory and maintained in Dr. Lianxiang Luo's laboratory at Guangdong Medical University. All mice were maintained and raised in standard conditions (temperature of 23 ± 2°C; an illumination of 12 hday^{-1}) with conventional diets and water in SPF rooms at the Institute of Laboratory Animal Center and the Ethics Committee of Jinan University or Guangdong Medical University. Animal studies are reported in compliance with the ARRIVE guidelines (Percie du Sert et al., 2020) and with the recommendations made by the *British Journal of Pharmacology* (Lilley et al., 2020) and approved by the Institutional Animal Care and Use Committee at Jinan University or Guangdong Medical University. Mice were killed by carbon dioxide inhalation followed by dislocation of the neck by trained personnel at the end of the experiment or when mice developed signs of severe illness.

2.12 | LPS/D-galactosamine induced acute liver injury model

Mice (4 per cage) were allowed to adapt to the SPF environment for 2 weeks. C57BL/6J WT female mice were randomly divided into four groups (n = 8 for each group): Control, LPS/D-galactosamine, LPS/D-galactosamine+JNUTS013 15 mgkg^{-1}, LPS/D-galactosamine+JNUTS013 30 mgkg^{-1}. The JNUTS013 injection solution was freshly prepared by mixing the DMSO stock solution (50 mM) with PEG300 (30%), Tween-80 (5%) and 0.9% sterile saline (various volumes based on the amount of JNUTS013 used). The LPS and D-galactosamine injection solution were also freshly prepared with sterile saline. JNUTS013 treatment groups were pretreated with intraperitoneal injection of JNUTS013 three times on the 1st, 4th and 7th day. During the JNUTS013 priming time, the control and LPS/D-galactosamine groups were administered with equal volume of saline intraperitoneally. On the 9th day, except for the control group, mice in other groups were injected intraperitoneally with LPS (100 μgkg^{-1}) and D-galactosamine (700 mgkg^{-1}) at the same time. All mice were killed after 5 h of injection by carbon dioxide inhalation

followed by dislocation of the neck. Serum, heart, liver, spleen, lung and kidney samples were collected and stored in liquid nitrogen for subsequent experiments.

2.13 | Dextran sulfate sodium salt (DSSS)-induced ulcerative colitis model

WT and *Nlrp3*$^{-/-}$ C57BL/6J female mice were randomly divided into three groups (n = 5 each group): Control, DSSS, DSSS+JNUTS013 30 mgkg^{-1}. Mice in the DSSS+JNUTS013 group were pretreated with freshly prepared JNUTS013 solution intraperitoneally once every other day for 1 week. During this period, other mice were administered with equal volume of saline solution intraperitoneally. From the 8th day, mice in DSSS and DSSS+JNUTS013 groups were administered with 3% DSSS (Gu et al., 2022) dissolved in drinking water for 1 week. At the same time, mice in the DSSS+JNUTS013 group were continuously administered JNUTS013 intraperitoneally once every other day for 1 week. At the end of treatment, mice were killed by carbon dioxide inhalation, serum, liver and colon samples were collected and stored in liquid nitrogen for future analysis. Body weight, water intake, faecal status and the disease activity index (DAI) of mice were recorded every day as described in Table 2.

2.14 | Colon tissue haematoxylin and eosin (H&E) staining

Mouse colon tissues were fixed in 4% paraformaldehyde at room temperature for 12 h. The tissues were embedded in paraffin, cut into 5-μm-thick sections, affixed onto glass slides, air dried at room temperature overnight and stored until usage. The slides were heated at 60°C for 1 h, immersed in xylene for 5 min and repeated five times followed by dehydration with ethanol gradient (100% ethanol 5 min twice, 90% ethanol 5 min, 80% ethanol 5 min, 70% ethanol 5 min and 50% ethanol for 5 min each), and gently rinse with tap water. The slides were then stained with haematoxylin and eosin using the immunohistochemistry kit (#D601037, Sangon Biotech, Shanghai, China) following the manufacturer's instructions. The histopathologic changes of colons were observed using an optical microscope (Olympus Optical Co, Tokyo, Japan).

2.15 | Measurement of serum aspartate aminotransferase (AST) and alanine aminotransferase (ALT) activities

Blood samples collected from mice were immediately centrifuged at 1000 g for 10 min at 4°C to obtain the sera and stored at −80°C. Liver tissues were weighed and added cold saline according to weight (g): volume (v) = 1:9 ratio, grinded and centrifugated at 10,000 *g* for 10 min at 4°C to obtain the supernatant. AST (Cat#C010-2-1) and ALT (Cat#C009-2-1) levels were determined using standard enzymatic assays (Jiancheng Bioengineering Institute, Jiangsu, China) according to the protocols.

2.16 | General synthetic methods of compounds JNUTS042-JNUTS046

The synthesis of compounds **JNUTS042-JNUTS046** followed the procedure report previously (Zhang, Wang, et al., 2022). First, 2,4-dimethylresorcinol (**2**) was prepared by reduction of 2,4-dihydroxy-3-methylbenzaldehyde (**1**) with $LiAlH_4$ at an atmosphere with argon. The aryl chloride was prepared by reaction of corresponding aromatic carboxylic acids with $SOCl_2$ in DMF. After the intermediates were collected, the aryl

esters could be easily formed by the intermediate (**2**) with aryl chloride, which undergoes Fries rearrangement to produce products **JNUTS042-JNUTS046** catalysed by $AlCl_3$ in dichloromethane. The products were purified by silica gel column chromatograph eluted with petroleum ether-ethyl acetate (from 10:1 to 6:1) and subsequent preparative HPLC eluted with MeOH-H_2O (80%).

(*E*)-1-(2,4-dihydroxy-3,5-dimethylphenyl)-3-(2-methoxyphenyl)-prop-2-en-1-one (**JNUTS042**). Pale yellow solid (30%). ^{1}H NMR (400 MHz, DMSO-d_6) δ 13.79 (1H, s), 8.15 (1H, d, *J* = 15.6 Hz), 8.02 (1H, d, *J* = 8.0 Hz), 7.93 (1H, d, *J* = 15.6 Hz), 7.92 (1H, s), 7.43 (1H, t, *J* = 8.0 Hz), 7.09 (1H, d, *J* = 8.0 Hz), 7.03 (1H, t, *J* = 8.0 Hz), 3.89 (3H, s), 2.20 (3H, s), 2.06 (3H, s). ^{13}C NMR (101 MHz, DMSO-d_6) δ 191.7, 162.3, 161.1, 158.2, 137.7, 132.3, 129.4, 128.3, 123.0, 120.8, 120.6, 116.2, 112.4, 111.8, 110.6, 55.7, 16.2, 8.3. HR-ESI-Q-TOF MS *m/z* calculated for $C_{18}H_{19}O_4$ $[M + H]^+$ 299.1283; found, 299.1288.

(*E*)-1-(2,4-dihydroxy-3,5-dimethylphenyl)-3-(3-methoxyphenyl)-prop-2-en-1-one (**JNUTS043**). Pale yellow solid (30%). ^{1}H NMR (400 MHz, DMSO-d_6) δ 13.75 (1H, s), 7.99 (1H, d, *J* = 15.6 Hz), 7.98 (1H, s), 7.76 (1H, d, *J* = 15.6 Hz), 7.48 (1H, d, 2.0), 7.46 (1H, d, *J* = 8.0 Hz), 7.37 (1H, t, *J* = 8.0 Hz), 7.02 (1H, dd, *J* = 8.0, 2.0 Hz), 3.83 (3H, s), 2.20 (3H, s), 2.06 (3H, s). 13C NMR (101 MHz, DMSO-d_6) δ 191.5, 162.3, 161.4, 159.7, 143.4, 136.1, 129.9, 129.6, 121.7, 121.6, 116.4, 116.3, 113.9, 112.3, 110.6, 55.3, 16.2, 8.2. HR-ESI-Q-TOF MS *m/z* calculated for $C_{18}H_{19}O_4$ $[M + H]^+$ 299.1283; found, 299.1283.

(*E*)-1-(2,4-dihydroxy-3,5-dimethylphenyl)-3-(2,3-methoxyphenyl)-prop-2-en-1-one (**JNUTS044**). Pale yellow solid (30%). ^{1}H NMR (400 MHz, DMSO-d_6) δ 13.71 (1H, s), 8.07 (1H, d, *J* = 15.6 Hz), 7.96 (1H, d, *J* = 15.6 Hz), 7.96 (1H, s), 7.70–7.67 (1H, m), 7.16–7.14 (2H, m), 3.84 (3H, s), 3.81 (3H, s), 2.20 (3H, s), 2.06 (3H, s). ^{13}C NMR (101 MHz, DMSO-d_6) δ 191.6, 162.2, 161.1, 152.8, 148.2, 137.3, 129.5, 128.2, 124.2, 122.1, 119.2, 116.2, 115.0, 112.3, 110.6, 61.1, 55.8, 16.1, 8.2. HR-ESI-Q-TOF MS *m/z* calculated for $C_{19}H_{21}O_5$ $[M + H]^+$ 329.1389; found, 329.1395.

(*E*)-1-(2,4-dihydroxy-3,5-dimethylphenyl)-3-(3,4-methoxyphenyl)-prop-2-en-1-one (**JNUTS045**). Pale yellow solid (30%). ^{1}H NMR (400 MHz, DMSO-d_6) δ 13.92 (1H, s), 7.94 (1H, s), 7.85 (1H, d, *J* = 15.2 Hz), 7.75 (1H, d, *J* = 15.2 Hz), 7.53 (1H, d, *J* = 1.2 Hz), 7.42 (1H, dd, *J* = 8.4, 1.2 Hz), 7.03 (1H, d, *J* = 8.4 Hz), 3.87 (3H, s), 3.82 (3H, s), 2.19 (3H, s), 2.04 (3H, s). ^{13}C NMR (101 MHz, DMSO-d_6) δ 191.3, 162.2 (×2), 151.3, 149.0, 143.8, 129.3, 127.6, 123.9, 118.8, 116.2, 112.1, 111.6, 111.3, 110.5, 55.9, 55.6, 16.3, 8.3. HR-ESI-Q-TOF MS *m/z* calculated for $C_{19}H_{21}O_5$ $[M + H]^+$ 329.1389; found, 329.1393.

(*E*)-1-(2,4-dihydroxy-3,5-dimethylphenyl)-3-(2,3,4-methoxyphenyl)-prop-2-en-1-one (**JNUTS046**). Pale yellow solid (30%). ^{1}H NMR (400 MHz, DMSO-d_6) δ 13.84 (1H, s), 7.98 (1H, d, *J* = 15.6 Hz), 7.91 (s, 1H), 7.86 (d, *J* = 15.6 Hz, 1H), 7.84 (d, *J* = 8.8 Hz, 1H), 6.92 (d, *J* = 8.8 Hz, 1H), 3.88 (3H, s), 3.87 (3H, s), 3.78 (s, 3H), 2.19 (s, 3H), 2.04 (s, 3H). ^{13}C NMR (101 MHz, DMSO-d_6) δ 191.4, 162.2, 161.3, 155.8, 153.1, 141.8, 137.6, 129.3, 123.4, 121.1, 119.5, 116.2, 112.2, 110.5, 108.4, 61.6, 60.5, 56.1, 16.2, 8.3. HR-ESI-Q-TOF MS *m/z* calculated for $C_{20}H_{23}O_6$ $[M + H]^+$ 359.1495; found, 359.1494.

2.17 | Data and statistical analysis

The data and statistical analysis comply with the recommendations of the *British Journal of Pharmacology* on experimental design and analysis in pharmacology (Curtis et al., 2022). The results are presented as mean and standard deviation from at least n = five individual values. Bar charts were presented when scatter plots did not reveal unusual or interesting aspects of the dataset. All statistical analyses were performed by the GraphPad Prism software version 9.0 (RRID:SCR_002798, GraphPad Software, CA, USA). When normalized control group was included to perform statistical analysis, non-parametric Mann–Whitney *U* test analysis was used. For non-normalized values, unpaired two-tailed Student's t test was conducted to determine the difference between the model group (i.e. cell cultures or mice with induced inflammation) and JNUTS013-treated (or other agents treated) group at the same experimental setting. One-way ANOVA with Tukey's test was applied to determine the difference in mouse body weight and disease activity index scores in Figure 6. Post hoc tests were conducted only if *F* in ANOVA achieved $P < 0.05$. Sample sizes subjected to statistical analysis are at least five animal per group (n = 5), where n = number of independent values. For all experiment, *P* values < 0.05 were considered statistically significant.

For all cell cultures and animal studies, groups were randomized before the initiation of treatment. Once the treatment was initiated, the researchers were not blinded as it required the management of specific chemical treatment (alone or in combination) for each group. No data or value were excluded unless the cells were contaminated, or mice were sick and died. For the mouse ulcerative colitis experiment, the DSSS group in WT mice had two mice terminated during the treatment due to sickness through carbon dioxide inhalation. Subsequently, two new mice were immediately added to this group, which resulted in sample collection for colon and liver at different time. Hence, colon images from only three mice were shown in Figure 6i. However, the statistical analysis was conducted from a total of five mice in this group as well. Western blotting band intensity was always normalized to the control group in the same blot. The number of mice was calculated using the G Power software (Faul et al., 2007) based on a preliminary experiment to determine the effect of JNUTS013 in mice. To achieve an effective size of 1.72 at a power of 0.80 and with *P* value <0.05, the number of mice for each group was determined to be five through a one-tailed effect direction calculation (i.e. the effect is as expected through preliminary test), which was used for the DSSS-induced ulcerative colitis study. For LPS/D-galactosamine study, three additional mice per group were added from preliminary experiment.

2.18 | Materials

JNUTS013 (≥98% purity) was synthesized in the Tang laboratory. Lipopolysaccharide (LPS, from *Escherichia coli* O111:B4) was purchased from Sigma-Aldrich (Cat#L2630, Steinheim, Germany). Dimethyl sulfoxide (DMSO) was purchased from Aladdin Bio-Chem Technology (Cat#67–68-5, Shanghai, China). D-galactosamine (D-galactosamine) was purchased from Sigma-Aldrich (Cat#G1639, Steinheim, Germany). Hydrocortisone (Cat#HY-N0583), curcumin (Cat#HY-N0005), rapamycin (Cat#HY-10219), MG132 (Cat#HY-13259), bortezomib (Cat#HY-10227), hydroxychloroquine (Cat#HY-W031727), leupeptin hemisulfate (Cat#HY-18234A), bafilomycin A1 (Cat#HY-100558), 3-

methyladenine (Cat#HY-19312), dextran sulfate sodium salt (DSSS, Cat#HY-116282B) and disuccinimidyl suberate (DSS) (Cat#HY-W019543) were purchased from MedChemExpress (Monmouth Junction, NJ, USA). Phorbol 12-myristate 13-acetate (PMA, Cat#S7791), nigericin sodium salt (Cat#S6653), cycloheximide (Cat#S7418) and Z-VAD-FMK (Cat#S7023) were purchased from Selleckchem (Houston, TX, USA). NP-40 lysis buffer (Cat#K1127) was purchased from Apexbio (Houston, TX, USA). NH_4Cl (Cat#A100621) was purchased from Sangon Biotech (Shanghai, China). β-Mercaptoethanol was from Thermo/Fisher (Cat#BP176100, Waltham, MA, USA). Details of other materials and suppliers are provided in the specific sections.

2.19 | Nomenclature of targets and ligands

Key protein targets and ligands in this article are hyperlinked to corresponding entries in the IUPHAR/BPS Guide to PHARMACOLOGY http://www.guidetopharmacology.org and are permanently achieved in the Concise Guide to PHARMACOLOGY 2021/22 (Alexander et al., 2021a,b).

3 | RESULTS

3.1 | Dose-dependent anti-inflammatory effect of JNUTS013

We recently reported the synthesis of several sorbicillinoid compounds that inhibited liposaccharide (LPS)-induced production of nitric oxide (**NO**) (Zhang, Wang, et al., 2022), a second messenger that indicates the activation of inflammation (Sharma et al., 2007). To further explore the anti-inflammatory effect and the underlying mechanism of these compounds, we focused on a top compound JNUTS013 (Figure 1a). We first show that JNUTS013 significantly suppressed LPS-induced NO release in mouse macrophage-like RAW264.7 and BV2 cell lines in a dose-dependent manner (Figure 1b). The effect of JNUTS013 was stronger than a positive anti-inflammation compound, **hydrocortisone** (Figure 1b). JNUTS013 at 20 μM for 24 h moderately reduced the viability of RAW264.7 and BV2 cells, but had no effect at 10 μM (Figure 1c). In contrast, JNUTS013 did not show cytotoxicity to human peripheral blood monocyte THP-1 cells even at 20 μM for 24 h (Figure S1a). These results suggest that JNUTS013 is relatively safe at 10 μM. Hence, we used concentrations at or below 10 μM of JNUTS013 for subsequent studies unless specified.

To understand how JNUTS013 inhibited NO production, we examined the protein level of iNOS, a key enzyme that catalyses the production of NO (Zamora et al., 2000). The results show that LPS treatment increased the level of iNOS, which was inhibited by JNUTS013 in a dose-dependent fashion in RAW264.7 and BV2 cells (Figure 1d,e,g,h). An increase in the level of phosphorylated IκB was also observed by LPS in both cell lines (Figure 1d,e,g,h). However, it was not affected by JNUTS013, indicating that this compound does not inhibit the activation of the upstream NF-κB pathway. Consistent with the general idea that human monocytes usually do not produce NO by LPS, we failed to detect NO release in THP-1 cells. Nevertheless, the results in RAW264.7 and BV2 cells demonstrate a strong anti-inflammatory potential of JNUTS013.

3.2 | Time-dependent anti-inflammatory effect of JNUTS013

Subsequently, we assessed the time-dependent effect of JNUTS013 on LPS-induced NO production and iNOS expression. At 6 h of treatment, JNUTS013 rarely inhibited or even slightly increased the protein level of iNOS in RAW164.7 and BV2 cells, respectively; however, at 12–24 h, JNUTS013 significantly inhibited iNOS levels in both cell lines (Figure 2a,b,e,f). The inhibitory effect of JNUTS013 at 12–24 h was comparable with another positive anti-inflammation control compound **curcumin** but stronger than hydrocortisone (Figure 2a,b,e,f). Consistent with the iNOS expression level, JNUTS013 suppressed LPS-induced NO production although the inhibition at 6 h was not significant in RAW264.7 cells (Figure 2c,g, *upper*). Again, the treatment regime did not inhibit cell viability (Figure 2c,g, *lower*).

The inconsistence between NO production and iNOS expression at 6 h might have resulted from differences in cellular response to protein expression and chemical production (NO). Although the protein level change (on iNOS) takes longer to show up, that of NO is likely rapid, leading to a difference between the iNOS protein level and NO production at the early time point. Nonetheless, the longer duration time points confirm a potent anti-inflammation activity of JNUTS013.

3.3 | JNUTS013 inhibited NLRP3 expression through proteasomal degradation

During analysis, we noticed that JUNTS013 dose- and time-dependently suppressed LPS-induced increase in the protein level of NLRP3, a key factor in activating inflammation (Kelley et al., 2019), in RAW264.7, BV2 and THP-1 cells (Figures 1, 2 and S1). Such an inhibition was not seen for other proteins like **COX-2** (Figure 1d), indicating that JNUTS013 did not non-selectively reduce the expression of any cellular proteins. These results suggest an exciting possibilty that JNUTS013 inhibits inflammation through downregulating NLRP3, which is different from currently known NLRP3 inhibitors that suppress its activity.

To confirm that JNUTS013 indeed induced downregulation of NLRP3 in an inflammatory setting, we co-treated RAW264.7 cells with LPS and the agonist ATP and examined the expression of NLRP3 and secretion of IL-1β. The results show that although LPS alone or LPS plus ATP resulted in a similar increase in the level of NLRP3, only the latter induced the release of IL-1β into the culture media (Figure 3a). These data are consistent with the idea that ATP promotes the activation of inflammation, but not the initial priming stage where the level of NLRP3 is increased by LPS. JNUTS013 suppressed the increase in NLRP3 caused by LPS or LPS plus ATP (Figure 3a). Importantly, JNUTS013 abolished the release of IL-1β in cells treated with LPS plus ATP (Figure 3a). These results support our conclusion that JNUTS013 inhibits inflammation through suppressing NLRP3 expression.

Hence, we decided to determine how exactly JNUTS013 inhibits NLRP3 expression. We first asked if JNUTS013 induces proteasome dependent NLRP3 degradation. To this end, we pre-treated cells with increasing concentrations of a specific proteasome inhibitor **bortezomib** in the presence of LPS and JNUTS013. Again, the LPS-induced increase in NLRP3 was inhibited by JNUTS013 (Figure 3b). However, prior treatment with bortezomib

prevented JNUTS013 from downregulating NLRP3 in a concentration-dependent manner (Figure 3b). Accordingly, the increase in the level of iNOS was partially rescued (Figure 3b). Bortezomib alone also increased the level of NLRP3 (Figure 3b). These results confirm proteasomal degradation in regulating the protein level of NLRP3 both under normal conditions and in the presence of JNUTS013.

In addition to proteasome, proteins could also undergo caspase- or lysosome-dependent degradation. We used small molecules to block caspase (Z-VAD), to activate autophagy (**rapamycin** also know as sirolimus) or to block the autophagy-lysosomal pathway (**hydroxychloroquine sulfate**, NH_4Cl, leupeptin hemisulfate, bafilomycin A1 and 3-methoxyamphetamine [3-MA]) and found that none of these agents prevented JNUTS013 from degrading NLRP3 in RAW264.7 or BV2 cells (Figure S2a–d), precluding the involvement of caspase or lysosome in degrading NLRP3 by JNUTS013.

If JNUTS013 induces NLRP3 degradation, it should affect the protein stability of NLRP3. Hence, we treated cells with **cycloheximide**, a protein synthesis inhibitor, to block the production of NLRP3 and assessed the protein decay over time. The results show that cycloheximide time-dependently reduced NLRP3 protein level (Figure 3c,d), consistent with the idea that NLRP3 undergoes protein degradation. Interestingly, JNUTS013 caused an even greater reduction in NLRP3 level than cycloheximide at later time point (Figure 3c,d), suggesting that JNUTS013 is a potent destabilizer for NLRP3. Co-treatment with JNUTS013 and cycloheximide caused less inhibition on NLRP3 than JNUTS013 alone, but more than cycloheximide alone (Figure 3c,d), probably because cycloheximide inhibited the translation of as-yet unidentified protein factors required for JNUTS013 to degrade NLRP3. The levels of other proteins such as **Chk1**, UHRF1 and phosphorylated **mTOR** did not follow that of NLRP3 (Figure 3c), reinforcing the idea that JNUTS013 does not induce degradation of any proteins.

The chemical structure of JNUTS013 resembles the so-called pan-assay interference compounds (PAINS) that may directly modify proteins. To determine if JNUTS013 induces NLRP3 degradation through directly modifying the protein (e.g. forming covalent bonds with NLRP3), we immunoprecipitated NLRP3 proteins from cultured BV2 cells and incubated with JNUTS013 *in vitro* over time. We did not observe any protein modification or level reduction of NLRP3 by JNUTS013 *in vitro*. In contrast, a known cross-linking agent, disuccinimidyl suberate (DSS) caused NLRP3 protein modification (Figure 3e). These results preclude the possibility that JNUTS013 directly modifies NLRP3 to induce its degradation, which in turn supports a signalling transduction-dependent mechanism (i.e. proteasome) in degrading NLRP3 by JNUTS013.

3.4 | JNUTS013 inhibits inflammatory gene expression

To confirm the anti-inflammatory effect of JNUTS013, we performed qPCR to measure the mRNA levels of inflammation genes including *Nlrp3*, *Pycard* (encoding ASC), *Il-1β*, Il-18, *Il-6*, *Cxcl10*, *Tnfα* and *Nos2* (encoding iNOS) in RAW264.7 cells. The results show that LPS increased the mRNA levels of all tested genes, although to different extents, for instance significantly on *Nlrp3* and *Nos2* but only weakly on *Pycard* (Figure 4a–l), consistent with the protein level increase of these genes. Although JNUTS013 significantly

suppressed the increases in downstream inflammatory genes, it did not inhibit that of *Nlrp3* (Figure 4a,b), supporting the concept that JNUTS013 induces proteasomal degradation, but not transcriptional inhibition of NLRP3. JNUTS013 did not noticeably reduce the level of *Pycard* either (Figure 4b), consistent with a much weak effect of JNUTS013 on ASC expression. JNUTS013 also did not significantly affect LPS-upregulated genes involved in inhibiting NF-κB (*Nfkbib*) or apoptosis (***Bcl2***) (Figure 4h,l), similar to its lack of effect on the p-IκB protein level (Figure 1d). These results suggest that JNUTS013 did not globally affect expression of genes involved in inflammation, but more specifically through the NLRP3 pathway.

We showed that JNUTS013 blocked the secretion of IL-1β by LPS and ATP (Figure 3a). To further determine if this is NLRP3 activation dependent, we measured the secreted protein levels of **TNFα** and IL-1β by ELISA. The results show that JNUTS013 effectively reduced TNFα and IL-1β secretion triggered by LPS in RAW264.7 cells, which was significantly reversed by a known agonist of the NLRP3 inflammasome, nigericin (Figure 4m,n), supporting that JNUTS013 inhibited the release of these inflammation factors through NLRP3.

3.5 | JNUTS013 inhibited ASC and NLRP3 oligomerization

As we observed a significant reduction in NLRP3 level by JNUTS013, we asked if JNUTS013 could suppress the formation of the NLRP3 inflammasome. For this purpose, we used DSS crosslinking to acquire ASC and NLRP3 oligomers from BV2 cells. The results show that LPS slightly increased the level of ASC monomer (Figure 4o), consistent with the about 1.5-fold increase in the mRNA level (Figure 4b). However, such an increase was reduced by JNUTS013 in a dose-dependent manner (Figure 4o). LPS alone did not significantly increase the level of ASC dimmer, which were actually increased by low dose of JNUTS013 but greatly suppressed by high dose of JNUTS013 (Figure 4o), indicating a dose-dependent suppression of ASC oligomerization. From the insoluble pellet that was supposed to contain the NLRP3 inflammasome, we observed an increase in the levels of NLRP3 monomer and possibly NLRP3-ASC-Caspase-1 heterodimer or heterotrimer by LPS (Figure 4o, lanes 1–2, I-III, respectively). These three bands recognized by the anti-NLRP3 antibody were all reduced by JNUTS013 dose-dependently (Figure 4o, lanes 2–4). In contrast, two of three non-specific low molecular weight bands were not affected by JNUTS013 (Figure 4o, asterisks), indicating that JNUTS013 specifically reduces high molecular weight bands (I-III) that are likely NLRP3 monomers/multimers. Although the total cellular level of NLRP3 was reduced by JNUTS013, that of ASC was not (Figure 4p), indicating that the reduced ASC monomer or dimer in the insoluble cell lysates might be due to less recruitment through reduced NLRP3. These results are similar to those from bone marrow derived macrophages, where LPS did not change ASC levels (Vijayaraj et al., 2021), supporting the idea that JNUTS013 mainly targets NLRP3 and weakly ASC for protein degradation, which leads to reduced NLRP3-ASC inflammasome assembly.

To verify these results in single cell levels, we performed antibody-based immunofluorescence to assess cellular expression of ASC and NLRP3. Under normal conditions, the level of NLRP3 in THP-1 cells was relatively low and it did not form clear

specks. However, LPS treatment increased the level of NLRP3 with specks forming in the cytoplasm around the nuclear envelop (Figure 5a). JNUTS013 significantly inhibited the increases in both the level and speck formation of NLRP3 induced by LPS (Figure 5a,b). LPS increased the level of ASC in THP-1 cells (Figure 5c) consistent with the western blotting results (Figure S1b,d), which was inhibited by JNUTS013 (Figure 5c,d). Unlike bulk immunoblotting results where no obvious changes in ASC levels were observed in BV2 cells (Figure 4p), immunofluorescence shows that LPS increased ASC levels in single cells, which was inhibited by JNUTS013 (Figure 5e,f). Further, the peri-nuclear localization of ASC was more evident in BV2 cells than in THP-1 cells. The discrepancies in ASC protein levels may reflect the differences in both cell lines and detection methods. Nonetheless, these results collectively show that JNUTS013 inhibited LPS-induced upregulation of NLRP3 and to a lesser degree ASC, supporting the anti-inflammatory effect of JNUTS013.

3.6 | JNUTS013 alleviated acute liver injury induced by LPS/D-galactosamine in C57 mice

To confirm the anti-inflammatory effect of JNUTS013 *in vivo*, we first explored the effect of JNUTS013 on LPS/D-galactosamine-induced acute liver injury in C57 wild type (WT) mice. Compared with the control group, LPS/D-galactosamine induced dramatic liver swelling (Figure 6a). JNUTS013 treatment inhibited liver swelling generally in a dose-dependent manner (Figure 6a). Consistently, LPS/D-galactosamine significantly increased liver weight (Figure 6b), which was moderately and significantly reduced by low and high doses of JNUTS013, respectively (Figure 6b).

To further determine the liver toxicity, we measured the enzymatic activities of aspartate aminotransferase (AST) and alanine aminotransferase (ALT), common indicators of liver injury, in the sera. The results show that LPS/D-galactosamine significantly increased the activities of ALT and AST in mice (Figure 6c,d), which were significantly inhibited by JNUTS013 in a dose-dependent manner (Figure 6c,d), demonstrating protection of mouse liver injury by JNUTS013. Like in cell cultures, LPS/D-galactosamine greatly increased the protein level of NLRP3 in mouse liver tissues, which was reduced by JNUTS013 (Figure 6e), suggesting that JNUTS013 also induces NLRP3 degradation *in vivo*.

3.7 | The anti-inflammatory effect of JNUTS013 depends on NLRP3

To further verify that NLRP3 is the molecular target by which JNUTS013 inhibits inflammation, we assessed ulcerative colitis from *Nlrp3*$^{+/+}$ and *Nlrp3*$^{-/-}$ mice. Sustained body weight loss, increased disease activity index score (determined according to parameters in Table 2) and reduced length of colon are typical features of ulcerative colitis in mice induced by 3% disuccinimidyl suberate salt (DSSS) (Jurjus et al., 2004). For *Nlrp3*$^{+/+}$ mice, compared with the control group with steady increase in body weight, DSSS treatment induced significant weight loss after 2 weeks (Figure 6f), which was significantly ameliorated by JNUTS013 (Figure 6f). *Nlrp3*$^{-/-}$ mice maintained their body weight in the absence of treatment but lost significantly when treated with DSSS (Figure 6g), similar to WT mice. However, JNUTS013 was not able to rescue the body weight loss in *Nlrp3*$^{-/-}$ mice (Figure 6g).

We then used the disease activity index score to assess mouse ulcerative colitis. DSSS treatment significantly increased the disease activity index score in both *Nlrp3*$^{+/+}$ and *Nlrp3*$^{-/-}$ mice (Figures 6h,i and S3), consistent with the induction of bowel inflammation. Although JNUTS013 significantly improved the disease activity index score in *Nlrp3*$^{+/+}$ mice, it did not show any protective effect in *Nlrp3*$^{-/-}$ mice (Figures 6h,i and S3). Other classical ulcerative colitis markers including the length and histopathology of the colon show that although JNUTS013 significantly restored the colon length and reduced the tissue injury induced by DSSS in *Nlrp3*$^{+/+}$ mice, the effect was moderate and not significant in *Nlrp3*$^{-/-}$ mice (Figures 6j,k and S4). Combined, these data strongly suggest that JNUTS013 exerted the anti-inflammatory activity by acting on NLRP3.

3.8 | The structure–activity relationship (SAR) of JNUTS013 in inhibiting NLRP3

We then decided to profile the structural features that determine the activity of JNUTS013 in degrading NLRP3. Representative monomeric sorbicillinoids consist of a methyl substituted resorcinol skeleton and a sorbyl side chain. Our studies demonstrated that substitution of (E)-3-phenyl-2-propenoyl side chains with fluoro and methoxy respectively, increased the anti-inflammation potency (Zhang, Wang, et al., 2022). In addition, a recent study showed that monomeric sorbicillinoid analogues with 4-methylresorcinol skeleton also exhibited strong anti-inflammatory effects (Zhang et al., 2019). Hence, to profile the structure–activity relationship and to further assess the contribution of methoxy to the anti-inflammatory potency of JNUTS013, we designed and successfully synthesized a series of sorbicillinoid analogues with different numbers of methoxy groups and at different locations in the side chain, as well as with different resorcinol skeletons (Figures S5 and S6).

We first evaluated the activities of these analogues on the level of NLRP3 at 10 μM, a concentration that was shown to be effective yet non-toxic for JNUTS013. We found that trimethoxy group substitutions at the 3″-, 4″- and 5″-positions of the right phenyl ring are most critical for inhibiting NLRP3 expression (Figure 7a–c). Mono- and dimethoxy group substitution or reposition of the trimethoxy groups dramatically lost the inhibition on NLRP3 expression (Figure 7a–c). In comparison with the right phenyl ring, substitution number of methyl and methoxy on the left phenyl ring had little to no effect (Figures 7a–c and S7). Consistent with the inhibition on NLRP3 expression, JNUTS013 and analogues with trimethoxy group substitutions at the 3″, 4 and 5″-positions of the right phenyl ring significantly inhibit LPS-induced iNOS protein expression and NO release (Figure 7b–e). However, some of the other compounds also suppressed LPS-induced iNOS increase and NO production (Figure 7a,d,e), indicating that they may inhibit inflammation independent of NLRP3 protein reduction. On the other hand, all compounds except JNUTS032 did not obviously inhibit cell survival even at 10 μM (Figure 7f), indicating weak cytotoxicity of these compounds.

To further test the structure–activity relationship activities, we selected several compounds with 0 (JNUTS008), 1 (JNUTS012), 2 (JNUTS045) or 3 (JNUTS013, 032 and 046) methoxy groups at the right phenyl ring. We found that only when the compound has three methoxy groups that are at the 3″-, 4″- and 5″-positions of the right phenyl ring, they can (JNUTS013 and 032) dose-dependently inhibit NLRP3 expression (Figure S7). Together,

these results suggest that JNUTS013-like compounds have the potential to be developed into anti-inflammation agents.

4 | DISCUSSION

NLRP3 inflammasome is activated by exogenous and endogenous stimuli to constitute an innate defence system. However, aberrant activation or gain-of-function mutations of NLRP3 lead to prolonged or chronic inflammation, contributing to various human diseases including arthritis, hereditary cryopyrin-associated periodic syndrome (CAPS), rheumatoid and osteoarthritis (Conforti-Andreoni et al., 2011). Therefore, the development of drugs that target the NLRP3 inflammasome has remained a hot research topic and many small molecule inhibitors have been developed to inhibit the activity of NLRP3 (Zahid et al., 2019). Here, we report exciting results on a recently synthesized compound, JNUTS013, in inhibiting inflammation through inducing proteasome-dependent degradation of NLRP3 both *in vitro* and *in vivo*, indicating an unique action that is distinct from previously reported NLRP3 inhibitors.

The compound under certain situations also inhibited the expression of ASC (apoptosis-associated speck-like protein containing a CARD; PYCARD), but the effect was much weaker and less stable than that on NLRP3. In contrast, JNUTS013 did not reduce the protein level of other proteins such as COX-2, Chk1 or UHRF1, suggesting that this compound does not non-selectively induce degradation of any proteins. Pretreatment with nigericin, an agonist of NLRP3, significantly prevented the inhibition of LPS-induced production of inflammatory cytokines by JNUTS013. Further, the compound failed to rescue bowel inflammation in *Nlrp3* knockout mice. These results confirm that the anti-inflammatory effect of JNUTS013 depends on NLRP3, but not through pleotropic effects. In addition, we showed that JNUTS013 does not seem to directly modify NLRP3 proteins, arguing against a model in which the compound covalently modifies NLRP3 like other pan-assay interfering compounds to cause their degradation. Together, our study shows a previously unrecognized action of chemicals that inhibit inflammation through inducing proteasomal degradation of NLRP3, representing an innovative strategy in targeting NLRP3 in treating inflammatory diseases.

At present, the precise molecular mechanisms by which JNUTS013 induce NLRP3 degradation remain unknown. A possibility is that the compound might bind to and recruit it to the proteasome in cells (not to covalently modify the protein though). Preliminary molecular docking analysis shows potential binding of JNUTS013 to Ala227, Ala228, Ile411, Val414, Thr439, Tyr443 and Tyr632 of NLRP3 with a docking score of $-7.7\ \text{kcalmol}^{-1}$ that is well below the commonly accepted threshold of $-5\ \text{kcalmol}^{-1}$. Nonetheless, this type of analysis does not constitute any solid evidence for a direct interaction of JNUTS013 with NLRP3. Further analyses are needed to address this issue in a future study.

The structure–activity relationship studies reveal two overlapping yet distinct aspects of the anti-inflammatory effects of JNUTS013-related compounds. On one hand, it seems to follow a strict structural requirement to induce NLRP3 degradation, among which trimethoxy group

substitutions at the 3″-, 4″- and 5″-positions of the right benzene ring are crucial. Mono- or di-methoxy groups at the 3″-, 4″-, and 5″ positions or trimethoxy groups but at 2″-, 3″- and 4″-positions showed much less effect. These results introduce valuable information about future detailed medicinal chemistry study to identify more potent compounds that degrade NLRP3. On the other hand, we noticed discrepancies between NLRP3 expression and the anti-inflammatory effects of these compounds. Even though some JNUTS013 analogues did not inhibit NLRP3 expression, they inhibited iNOS expression and NO release. These results suggest that the structural backbone of JNUTS013 is probably sufficient to inhibit the inflammation, although they may not necessarily depend on the induction of NLRP3 degradation. Again, more thorough medicinal chemistry studies are needed to solve this conundrum.

5 | CONCLUSION

Here, we report the functional characterization of a new compound JNUTS013 in inhibiting inflammation through inducing proteasome-dependent degradation of NLRP3 *in vitro* and *in vivo*. Our structure–activity relationship studies determined the importance of the structure of JNUTS013 in inhibiting NLRP3 inhibition and inflammation. Overall, our work provided strong evidence to support the development of an innovative approach in the treatment of inflammatory diseases by chemically inducing protein degradation of NLRP3.

Supplementary Material

Refer to Web version on PubMed Central for supplementary material.

ACKNOWLEDGEMENTS

This work was supported by National Key Research and Development Program of China (2022YFC2804100 and 2018YFC0311000) to Jinshan Tang.

DATA AVAILABILITY STATEMENT

All data supporting the findings of this study are available within the paper or its supplementary information and are available from the corresponding author upon reasonable request.

Abbreviations:

ALT	alanine aminotransferase
ASC	apoptosis-associated speck-like protein containing a CARD; PYCARD)
AST	aspartate aminotransferase
DSS	disuccinimidyl suberate
DSSS	dextran sulfate sodium salt
MTT	3-(4,5-Dimethylthiazol-2-yl)-2,5-diphenyltetrazolium bromide

SDS-PAGE sodium dodecyl sulphate-polyacrylamide gel electrophoresis

REFERENCES

Alexander SP, Fabbro D, Kelly E, Mathie A, Peters JA, Veale EL, Armstrong JF, Faccenda E, Harding SD, Pawson AJ, Southan C, Davies JA, Beuve A, Brouckaert P, Bryant C, Burnett JC, Farndale RW, Friebe A, Garthwaite J, … Waldman SA (2021a). THE CONCISE GUIDE TO PHARMACOLOGY 2021/22: Catalytic receptors. British Journal of Pharmacology, 178(S1), S264–S312. 10.1111/bph.15541 [PubMed: 34529829]

Alexander SP, Fabbro D, Kelly E, Mathie A, Peters JA, Veale EL, Armstrong JF, Faccenda E, Harding SD, Pawson AJ, Southan C, Davies JA, Boison D, Burns KE, Dessauer C, Gertsch J, Helsby NA, Izzo AA, Koesling D, … Wong SS (2021b). THE CONCISE GUIDE TO PHARMACOLOGY 2021/22: Enzymes. British Journal of Pharmacology, 178(S1), S313–S411. 10.1111/bph.15542 [PubMed: 34529828]

Alexander SPH, Roberts RE, Broughton BRS, Sobey CG, George CH, Stanford SC, Cirino G, Docherty JR, Giembycz MA, Hoyer D, Insel PA, Izzo AA, Ji Y, MacEwan DJ, Mangum J, Wonnacott S, & Ahluwalia A (2018). Goals and practicalities of immunoblotting and immunohistochemistry: A guide for submission to the British Journal of Pharmacology. British Journal of Pharmacology, 175, 407–411. 10.1111/bph.14112 [PubMed: 29350411]

Brough D, Pelegrin P, & Nickel W (2017). An emerging case for membrane pore formation as a common mechanism for the unconventional secretion of FGF2 and IL-1beta. Journal of Cell Science, 130, 3197–3202. 10.1242/jcs.204206 [PubMed: 28871048]

Broz P, & Dixit VM (2016). Inflammasomes: Mechanism of assembly, regulation and signalling. Nature Reviews Immunology, 16, 407–420. 10.1038/nri.2016.58

Coll RC, Robertson AA, Chae JJ, Higgins SC, Munoz-Planillo R, Inserra MC, Vetter I, Dungan LS, Monks BG, Stutz A, & Croker DE (2015). A small-molecule inhibitor of the NLRP3 inflammasome for the treatment of inflammatory diseases. Nature Medicine, 21, 248–255. 10.1038/nm.3806

Conforti-Andreoni C, Ricciardi-Castagnoli P, & Mortellaro A (2011). The inflammasomes in health and disease: From genetics to molecular mechanisms of autoinflammation and beyond. Cellular & Molecular Immunology, 8, 135–145. 10.1038/cmi.2010.81 [PubMed: 21258359]

Curtis MJ, Alexander SPH, Cirino G, George CH, Kendall DA, Insel PA, Izzo AA, Ji Y, Panettieri RA, Patel HH, Sobey CG, Stanford SC, Stanley P, Stefanska B, Stephens GJ, Teixeira MM, Vergnolle N, & Ahluwalia A (2022). Planning experiments: Updated guidance on experimental design and analysis and their reporting III. British Journal of Pharmacology, 179, 3907–3913. 10.1111/bph.15868 [PubMed: 35673806]

Dekker C, Mattes H, Wright M, Boettcher A, Hinniger A, Hughes N, Kapps-Fouthier S, Eder J, Erbel P, Stiefl N, Mackay A, & Farady CJ (2021). Crystal structure of NLRP3 NACHT domain with an inhibitor defines mechanism of Inflammasome inhibition. Journal of Molecular Biology, 433, 167309. 10.1016/j.jmb.2021.167309 [PubMed: 34687713]

Dick MS, Sborgi L, Ruhl S, Hiller S, & Broz P (2016). ASC filament formation serves as a signal amplification mechanism for inflammasomes. Nature Communications, 7, 11929. 10.1038/ncomms11929

Ding W, Wang F, Li Q, Xue Y, Dong Z, Tian D, Chen M, Zhang Y, Hong K, & Tang J (2021). Isolation and characterization of anti-inflammatory sorbicillinoids from the mangrove-derived fungus Penicillium sp. DM815. Chemistry & Biodiversity, 18, e2100229. 10.1002/cbdv.202100229 [PubMed: 34085751]

Faul F, Erdfelder E, Lang AG, & Buchner A (2007). G*power 3: A flexible statistical power analysis program for the social, behavioral, and biomedical sciences. Behavior Research Methods, 39, 175–191. 10.3758/BF03193146 [PubMed: 17695343]

Geng X, Wang F, Tian D, Huang L, Streator E, Zhu J, Kurihara H, He R, Yao X, Zhang Y, & Tang J (2020). Cardiac glycosides inhibit cancer through Na/K-ATPase-dependent cell death induction. Biochemical Pharmacology, 182, 114226. 10.1016/j.bcp.2020.114226 [PubMed: 32976831]

Gu W, Zhang L, Han T, Huang H, & Chen J (2022). Dynamic changes in gut microbiome of ulcerative colitis: Initial study from animal model. Journal of Inflammation Research, 15, 2631–2647. 10.2147/JIR.S358807 [PubMed: 35494313]

Guo C, Fu R, Wang S, Huang Y, Li X, Zhou M, Zhao J, & Yang N (2018). NLRP3 inflammasome activation contributes to the pathogenesis of rheumatoid arthritis. Clinical and Experimental Immunology, 194, 231–243. 10.1111/cei.13167 [PubMed: 30277570]

Halle A, Hornung V, Petzold GC, Stewart CR, Monks BG, Reinheckel T, Fitzgerald KA, Latz E, Moore KJ, & Golenbock DT (2008). The NALP3 inflammasome is involved in the innate immune response to amyloid-beta. Nature Immunology, 9, 857–865. 10.1038/ni.1636 [PubMed: 18604209]

Heneka MT, Kummer MP, Stutz A, Delekate A, Schwartz S, Vieira-Saecker A, Griep A, Axt D, Remus A, Tzeng TC, Gelpi E, Halle A, Korte M, Latz E, & Golenbock DT (2013). NLRP3 is activated in Alzheimer's disease and contributes to pathology in APP/PS1 mice. Nature, 493, 674–678. 10.1038/nature11729 [PubMed: 23254930]

Hochheiser IV, Pilsl M, Hagelueken G, Moecking J, Marleaux M, Brinkschulte R, Latz E, Engel C, & Geyer M (2022). Structure of the NLRP3 decamer bound to the cytokine release inhibitor CRID3. Nature, 604, 184–189. 10.1038/s41586-022-04467-w [PubMed: 35114687]

Jin Y, & Fu J (2019). Novel insights into the NLRP 3 Inflammasome in atherosclerosis. Journal of the American Heart Association, 8, e012219. 10.1161/JAHA.119.012219 [PubMed: 31184236]

Jurjus AR, Khoury NN, & Reimund JM (2004). Animal models of inflammatory bowel disease. Journal of Pharmacological and Toxicological Methods, 50, 81–92. 10.1016/j.vascn.2003.12.002 [PubMed: 15385082]

Kelley N, Jeltema D, Duan Y, & He Y (2019). The NLRP3 Inflammasome: An overview of mechanisms of activation and regulation. International Journal of Molecular Sciences, 20, 3328. 10.3390/ijms20133328 [PubMed: 31284572]

Laliberte RE, Perregaux DG, Hoth LR, Rosner PJ, Jordan CK, Peese KM, Eggler JF, Dombroski MA, Geoghegan KF, & Gabel CA (2003). Glutathione s-transferase omega 1–1 is a target of cytokine release inhibitory drugs and may be responsible for their effect on interleukin-1beta posttranslational processing. The Journal of Biological Chemistry, 278, 16567–16578. 10.1074/jbc.M211596200 [PubMed: 12624100]

Lilley E, Stanford SC, Kendall DE, Alexander SPH, Cirino G, Docherty JR, George CH, Insel PA, Izzo AA, Ji Y, Panettieri RA, Sobey CG, Stefanska B, Stephens G, Teixeira M, & Ahluwalia A (2020). ARRIVE 2.0 and the British Journal of Pharmacology: Updated guidance for 2020. British Journal of Pharmacology, 177, 3611–3616. 10.1111/bph.15178 [PubMed: 32662875]

Liu X, Yin L, Shen S, & Hou Y (2021). Inflammation and cancer: Paradoxical roles in tumorigenesis and implications in immunotherapies. Genes & Diseases. 10.1016/j.gendis.2021.09.006

Lu A, Magupalli VG, Ruan J, Yin Q, Atianand MK, Vos MR, Schröder GF, Fitzgerald KA, Wu H, & Egelman EH (2014). Unified polymerization mechanism for the assembly of ASC-dependent inflammasomes. Cell, 156, 1193–1206. 10.1016/j.cell.2014.02.008 [PubMed: 24630722]

Magupalli VG, Negro R, Tian Y, Hauenstein AV, Di Caprio G, Skillern W, Deng Q, Orning P, Alam HB, Maliga Z, & Sharif H (2020). HDAC6 mediates an aggresome-like mechanism for NLRP3 and pyrin inflammasome activation. Science, 369, eaas8995. 10.1126/science.aas8995

Mayca Pozo F, Geng X, Tamagno I, Jackson MW, Heimsath EG, Hammer JA, Cheney RE, & Zhang Y (2021). MYO10 drives genomic instability and inflammation in cancer. Science Advances, 7, eabg6908. 10.1126/sciadv.abg6908 [PubMed: 34524844]

McAllister MJ, Chemaly M, Eakin AJ, Gibson DS, & McGilligan VE (2018). NLRP3 as a potentially novel biomarker for the management of osteoarthritis. Osteoarthritis and Cartilage, 26, 612–619. 10.1016/j.joca.2018.02.901 [PubMed: 29499288]

Ohto U, Kamitsukasa Y, Ishida H, Zhang Z, Murakami K, Hirama C, Maekawa S, & Shimizu T (2022). Structural basis for the oligomerization-mediated regulation of NLRP3 inflammasome activation. Proceedings of the National Academy of Sciences of the United States of America, 119, e2121353119. 10.1073/pnas.2121353119 [PubMed: 35254907]

Olcum M, Tastan B, Kiser C, Genc S, & Genc K (2020). Microglial NLRP3 inflammasome activation in multiple sclerosis. Advances in Protein Chemistry and Structural Biology, 119, 247–308. 10.1016/bs.apcsb.2019.08.007 [PubMed: 31997770]

Percie du Sert N, Hurst V, Ahluwalia A, Alam S, Avey MT, Baker M, Browne WJ, Clark A, Cuthill IC, Dirnagl U, Emerson M, Garner P, Holgate ST, Howells DW, Karp NA, Lazic SE, Lidster K, MacCallum CJ, Macleod M, … Würbel H (2020). The ARRIVE guidelines 2.0: Updated guidelines for reporting animal research. British Journal of Pharmacology, 177, 3617–3624. 10.1111/bph.15193 [PubMed: 32662519]

Pirzada RH, Javaid N, & Choi S (2020). The roles of the NLRP3 Inflammasome in neurodegenerative and metabolic diseases and in relevant advanced therapeutic interventions. Genes (Basel), 11, 131. 10.3390/genes11020131 [PubMed: 32012695]

Rathinam VA, Vanaja SK, & Fitzgerald KA (2012). Regulation of inflammasome signaling. Nature Immunology, 13, 333–342. 10.1038/ni.2237 [PubMed: 22430786]

Shalapour S, & Karin M (2015). Immunity, inflammation, and cancer: An eternal fight between good and evil. The Journal of Clinical Investigation, 125, 3347–3355. 10.1172/JCI80007 [PubMed: 26325032]

Sharma JN, Al-Omran A, & Parvathy SS (2007). Role of nitric oxide in inflammatory diseases. Inflammopharmacology, 15, 252–259. 10.1007/s10787-007-0013-x [PubMed: 18236016]

Swanson KV, Deng M, & Ting JP (2019). The NLRP3 inflammasome: Molecular activation and regulation to therapeutics. Nature Reviews Immunology, 19, 477–489. 10.1038/s41577-019-0165-0

Tian D, Tang J, Geng X, Li Q, Wang F, Zhao H, Narla G, Yao X, & Zhang Y (2020). Targeting UHRF1-dependent DNA repair selectively sensitizes KRAS mutant lung cancer to chemotherapy. Cancer Letters, 493, 80–90. 10.1016/j.canlet.2020.08.008 [PubMed: 32814087]

Vijayaraj SL, Feltham R, Rashidi M, Frank D, Liu Z, Simpson DS, Ebert G, Vince A, Herold MJ, Kueh A, Pearson JS, Dagley LF, Murphy JM, Webb AI, Lawlor KE, & Vince JE (2021). The ubiquitylation of IL-1β limits its cleavage by caspase-1 and targets it for proteasomal degradation. Nature Communications, 12, 2713. 10.1038/s41467-021-22979-3

Walsh D, McCarthy J, O'Driscoll C, & Melgar S (2013). Pattern recognition receptors--molecular orchestrators of inflammation in inflammatory bowel disease. Cytokine & Growth Factor Reviews, 24, 91–104. 10.1016/j.cytogfr.2012.09.003 [PubMed: 23102645]

Wang F, Jin S, Mayca Pozo F, Tian D, Tang X, Dai Y, Yao X, Tang J, & Zhang Y (2022). Chemical screen identifies shikonin as a broad DNA damage response inhibitor that enhances chemotherapy through inhibiting ATM and ATR. Acta Pharmaceutica Sinica B, 12, 1339–1350. 10.1016/j.apsb.2021.08.025 [PubMed: 35530159]

Wang F, Mayca Pozo F, Tian D, Geng X, Yao X, Zhang Y, & Tang J (2020). Shikonin inhibits cancer through P21 upregulation and apoptosis induction. Frontiers in Pharmacology, 11, 861. 10.3389/fphar.2020.00861 [PubMed: 32581812]

Wang X, Chi J, Huang D, Ding L, Zhao X, Jiang L, Yu Y, & Gao F (2020). Alpha-synuclein promotes progression of Parkinson's disease by upregulating autophagy signaling pathway to activate NLRP3 inflammasome. Experimental and Therapeutic Medicine, 19, 931–938. 10.3892/etm.2019.8297 [PubMed: 32010254]

Wicherska-Pawlowska K, Wrobel T, & Rybka J (2021). Toll-like receptors (TLRs), NOD-like receptors (NLRs), and RIG-I-like receptors (RLRs) in innate immunity. TLRs, NLRs, and RLRs ligands as immunotherapeutic agents for hematopoietic diseases. International Journal of Molecular Sciences, 22, 24. 10.3390/ijms222413397

Zahid A, Li B, Kombe AJK, Jin T, & Tao J (2019). Pharmacological inhibitors of the NLRP3 inflammasome. Frontiers in Immunology, 10, 2538. 10.3389/fimmu.2019.02538 [PubMed: 31749805]

Zamora R, Vodovotz Y, & Billiar TR (2000). Inducible nitric oxide synthase and inflammatory diseases. Molecular Medicine, 6, 347–373. 10.1007/BF03401781 [PubMed: 10952018]

Zhang L, Geng X, Wang F, Tang J, Ichida Y, Sharma A, Jin S, Chen M, Tang M, Pozo FM, Wang W, Wang J, Wozniak M, Guo X, Miyagi M, Jin F, Xu Y, Yao X, & Zhang Y (2022). 53BP1 regulates heterochromatin through liquid phase separation. Nature Communications, 13, 360. 10.1038/s41467-022-28019-y

Zhang M, Wang F, Ding W, Xu Z, Li X, Tian D, Zhang Y, & Tang J (2022). Synthesis of sorbicillinoid analogues with anti-inflammation activities. Bioorganic & Medicinal Chemistry, 54, 116589. 10.1016/j.bmc.2021.116589 [PubMed: 34971877]

Zhang P, Deng Y, Lin X, Chen B, Li J, Liu H, Chen S, & Liu L (2019). Anti-inflammatory mono- and dimeric sorbicillinoids from the marine-derived fungus *Trichoderma reesei* 4670. Journal of Natural Products, 82, 947–957. 10.1021/acs.jnatprod.8b01029 [PubMed: 30920218]

What is already known

- NLRP3 is a key inflammatory factor and an important target in human inflammatory diseases.
- NLRP3 inhibitors currently under development target the signaling pathway.

What does this study add

- Characterized a novel compound that inhibits inflammation through inducing NLRP3 protein degradation.
- The anti-inflammation effect of this compound depends on NLRP3 *in vitro* and *in vivo*.

What is the clinical significance

- Inhibiting NLRP3 through inducing its degradation expands our toolkits to treat inflammatory diseases.
- The structure-activity relationship allows future studies to identify more potent agents targeting NLRP3 in inflammation.

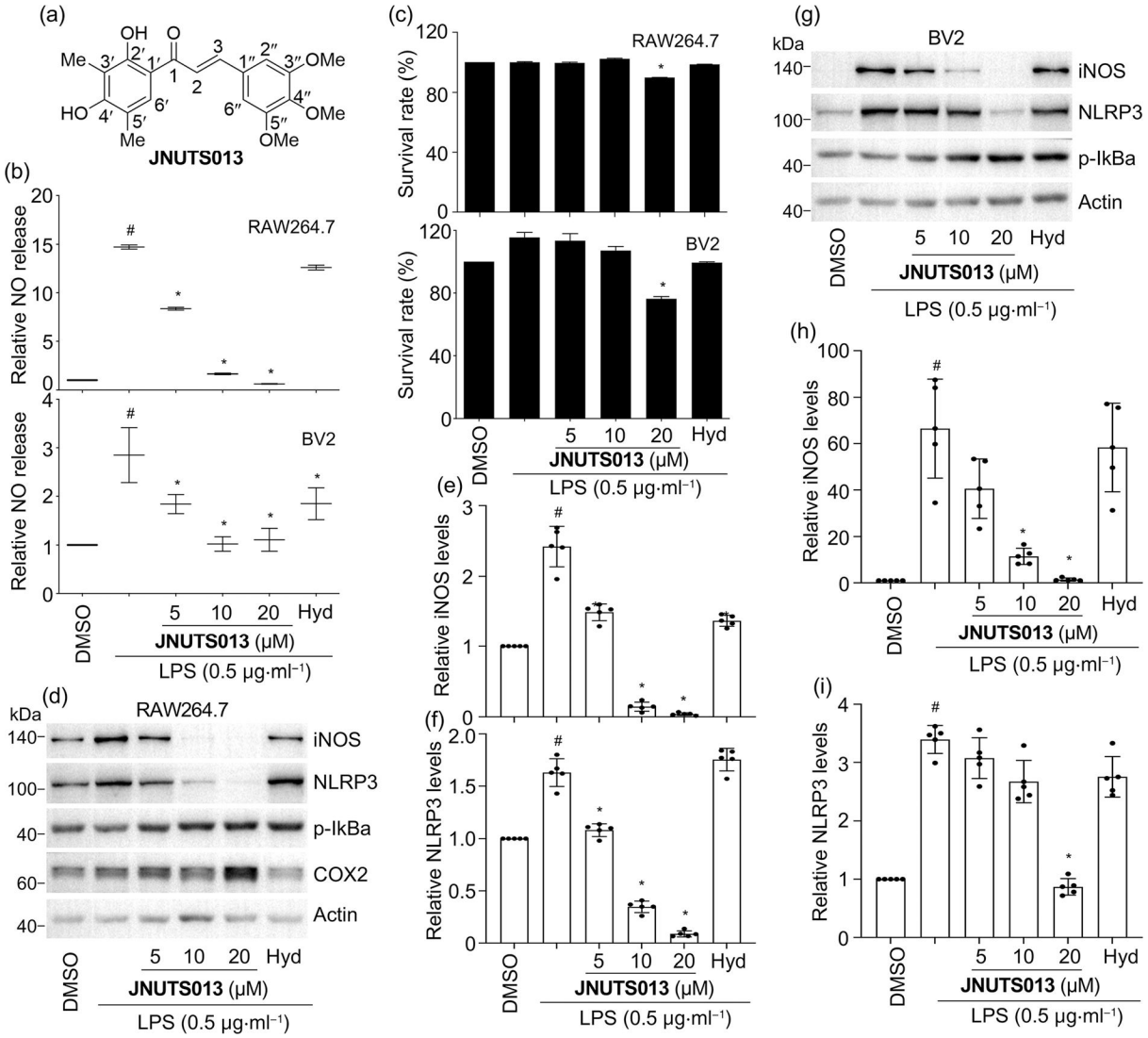

FIGURE 1.

JNUTS013 suppressed LPS-induced inflammatory protein expression and NO release in a dose-dependent manner. (a) Chemical structure of JNUTS013. RAW264.7 or BV2 cells were treated with LPS, JNUTS013 or hydrocortisone (Hyd) (20 μM) for 24 h, and measured (b) relative NO release, (c) relative cell survival ratio and (d, g) inflammatory protein levels. (e, f, h, i) Quantitation of protein levels of iNOS and NLRP3 from (d) and (g), respectively, was done by Image J. Data represent mean and standard deviation of levels normalized to the DMSO control group from n = 5 values. $^{\#}P < 0.05$ compared with the DMSO group, whereas $^{*}P < 0.05$ was compared with LPS treatment alone group by non-parametric analysis using prism 9.0. The Y axis represents values of the fold matched control. Bar charts are presented when there were no unusual aspects of data revealed by scatter plots.

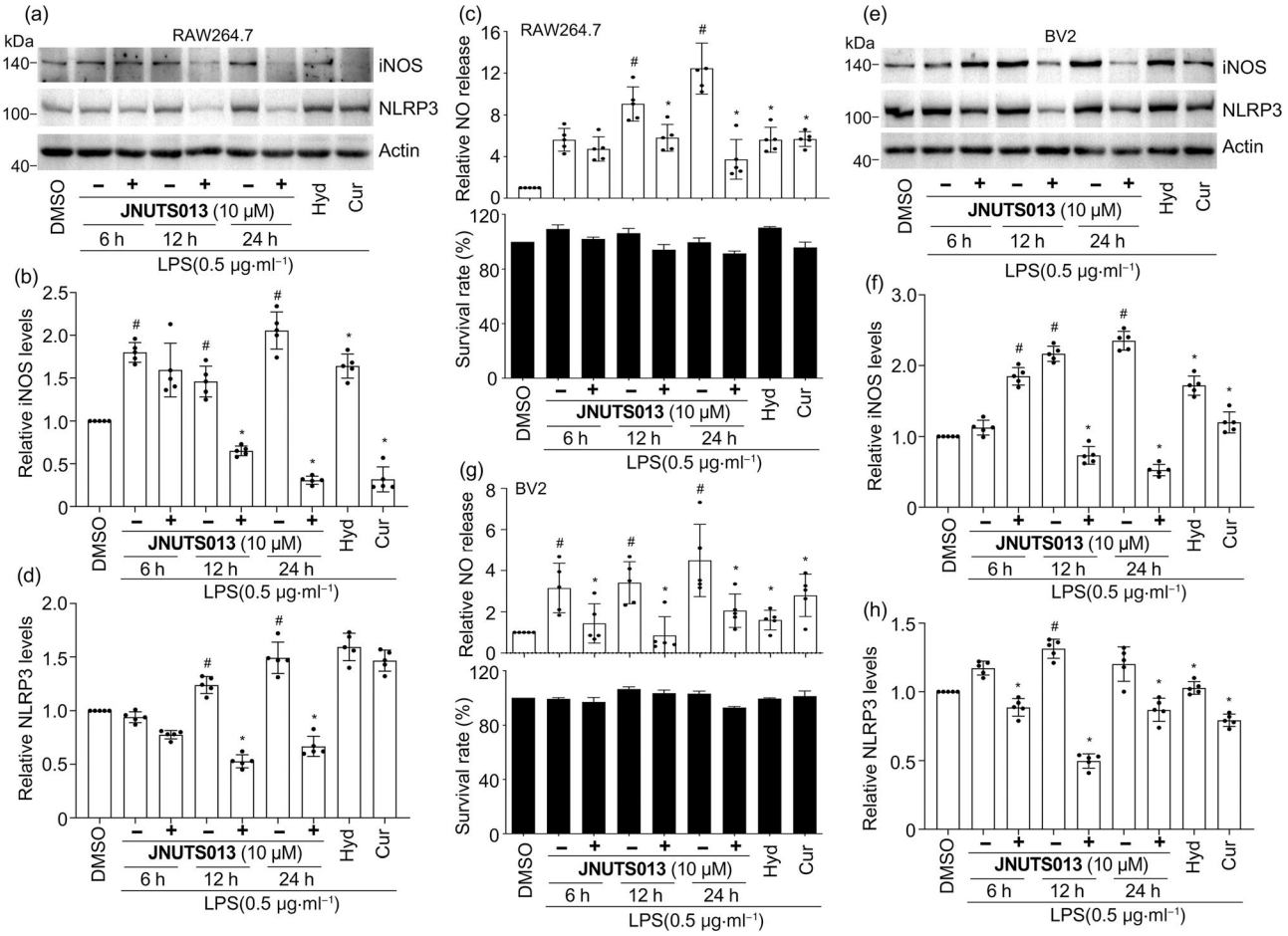

FIGURE 2.

Time-dependent inhibition of LPS-induced inflammatory protein expression and NO release by JNUTS013. RAW264.7 or BV2 cells were treated with LPS, JNUTS013, 20 μM of hydrocortisone (Hyd) or curcumin (cur) for 6–24 h and measured (a, e) inflammatory protein expression levels, (b, d, f, h) quantitation of protein levels of NLRP3 and iNOS in RAW264.7 and BV2 cells from (a) and (e), respectively and (c) and (g) relative NO release (*upper*) and cell survival (*lower*). Data represent mean and standard deviation normalized to that in the DMSO control group from at least five replicates. $^{\#}P < 0.05$ compared with the DMSO group, whereas $^{*}P < 0.05$ was compared with LPS treatment alone group by non-parametric analysis using Prism 9.0. The Y axis represents values of the fold matched control. Bar charts are presented when there were no unusual aspects of data revealed by scatter plots.

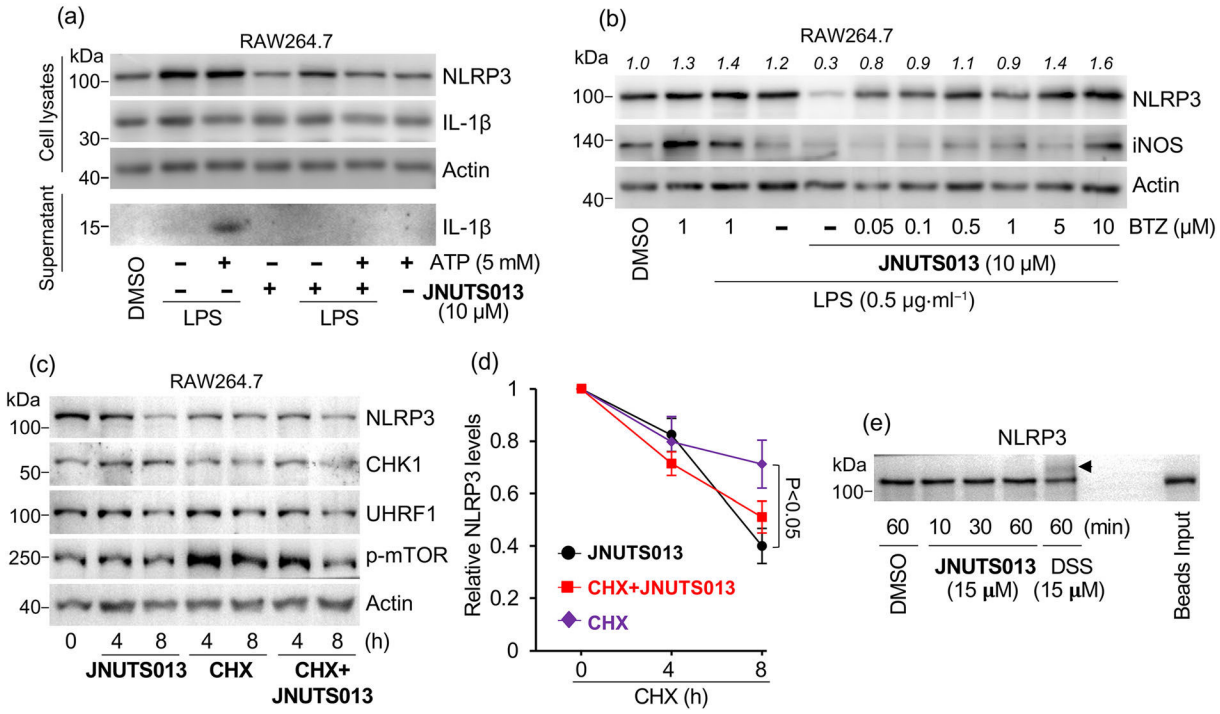

FIGURE 3.

JNUTS013 promoted proteasome-dependent degradation of NLRP3. (a) RAW264.7 cells were treated with 0.5 μgml^{-1} LPS for 24 h with or without 10 μM JNUTS013. ATP was added to the culture media at the last hour at a final concentration of 5 mM and protein expression was measured. Parallel cell culture media were collected and precipitated as described in the methods to detect the level of IL-1β. (b) RAW264.7 cells were treated with 0.5 μgml^{-1} LPS for 5.5 h, added different concentrations of bortezomib (BTZ) alone or with LPS for 30 min and then added 10 μM JNUTS013 for another 6 h. Protein expression was analysed. Quantitation of the protein band of NLRP3 represents mean from five values. (c) RAW264.7 cells were treated with 320 μM cycloheximide (CHX), 10 μM JNUTS03 or both and protein expression was examined. (d) Quantitation of the protein band of NLRP3 in RAW264.7 cells from (c). (e) Detection of NLRP3 modification by JNUTS013 or DSS *in vitro* as described in the methods. The arrow indicates modified NLRP3 proteins. Data represent mean and standard deviation from five values. Statistical analysis was conducted by prism 9.0 to indicate the difference between CHX and JNUTS013 at 8 h. The Y axis represents values of the fold matched control.

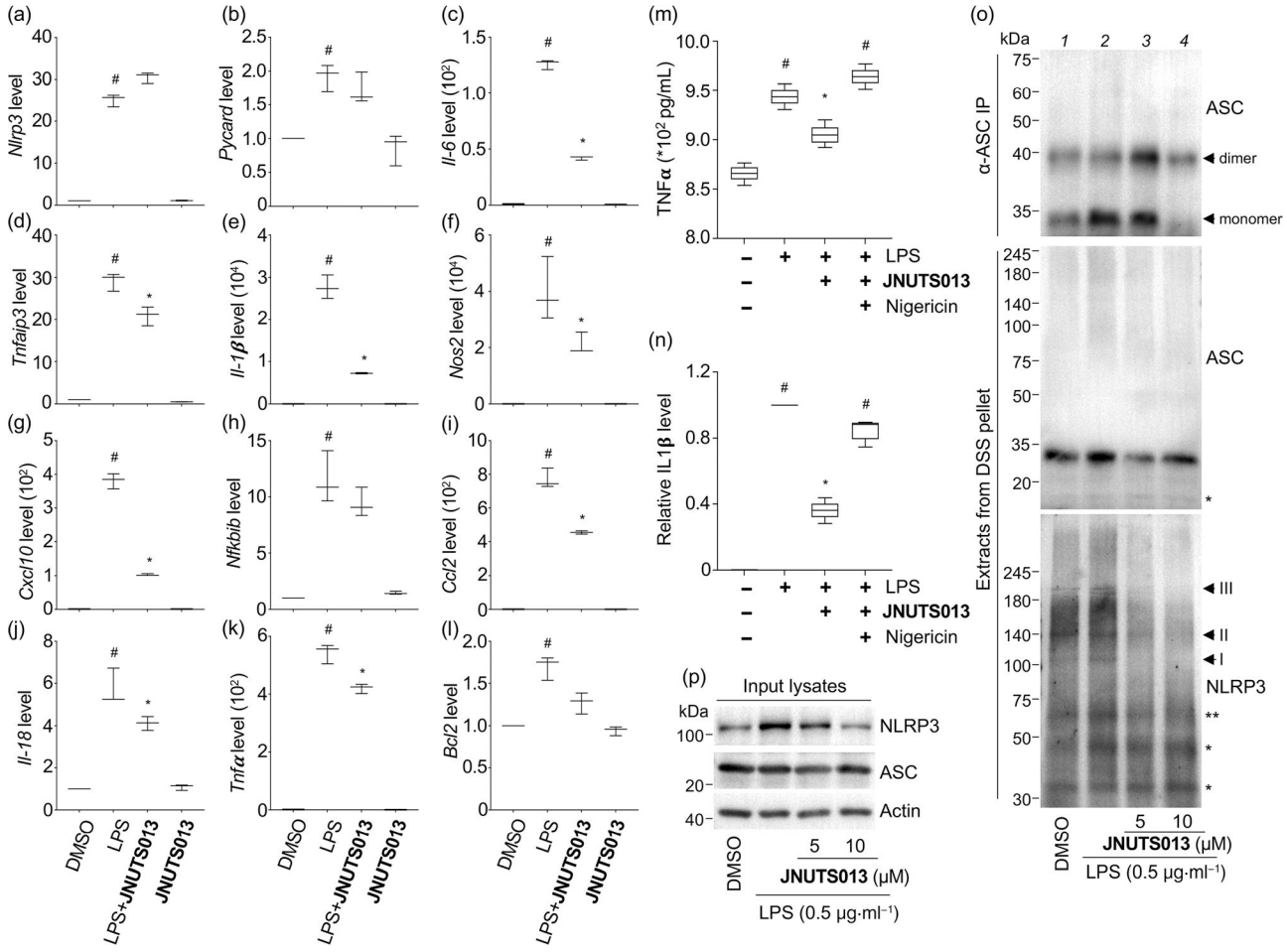

FIGURE 4.

JNUTS013 inhibited the inflammasome assembly and downstream inflammatory response. For qPCR analysis, RAW264.7 cells were treated with 10 μM JNUTS013, 0.5 μgml^{-1} LPS or the combination for 12 h, RNA was isolated and expression levels of genes including *Nlrp3* (a), *Pycard* (b), *Il6* (c), *Tnfaip3* (d), *Il1β* (e), *Nos2* (f), *Cxcl10* (g), *Nfkbib* (h), *Ccl2* (i), *Il18* (j), *Tnfα* (k) and *Bcl2* (l) were analysed. The protein levels of TNF-α (m) and IL-1β (n) in RAW264.7 cell culture media were examined by ELISA, in which relative levels of IL-1β were determined by normalizing to the LPS group. (o) NLRP3 and ASC oligomerization in lysates from BV2 cells pretreated with LPS and with different concentrations of JNUTS013 and collected by disuccinimidyl suberate (DSS) crosslinking. *Bands show non-specific bands not affected by JNUTS013 treatment, whereas **band was slightly reduced, although their identifies remain unknown at this moment. (p) Protein expression levels in whole cell lysates from BV2 cells. Data represent mean and standard deviation. $^{\#}P < 0.05$ compared with the DMSO group, whereas $^{*}P < 0.05$ was compared with LPS treatment alone group by non-parametric analysis using prism 9.0. The Y axis represents values of the fold matched control. Bar charts are presented when there were no unusual aspects of data revealed by scatter plots.

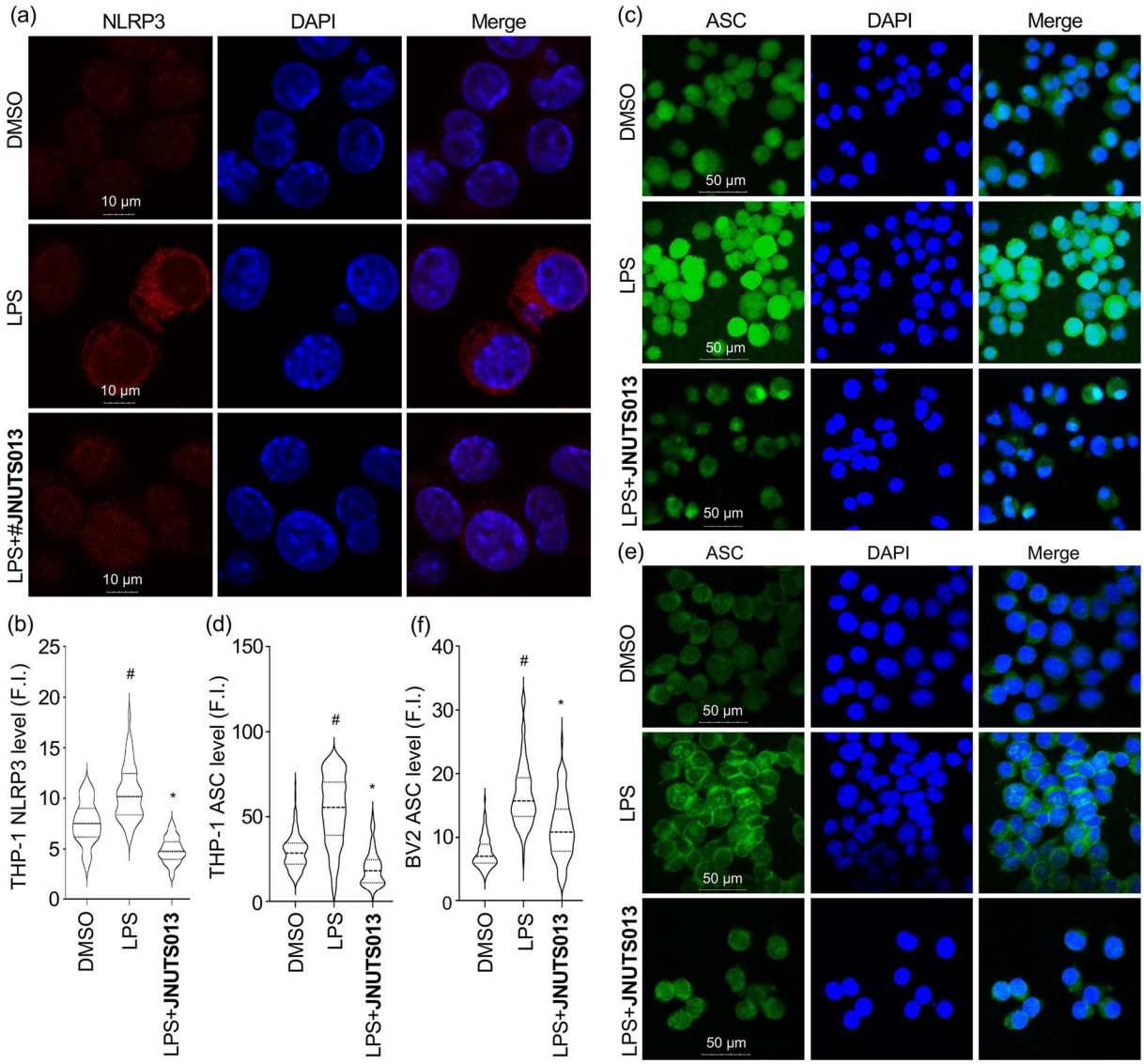

FIGURE 5.

JNUTS013 inhibited the upregulation and speck formation of NLRP3 and ASC in response to inflammation stimulation. THP-1 cells were treated with LPS (0.5 μgml^{-1}) and JNUTS013 (10 μM) for 12 h, fixed and stained for NLRP3 (a) or ASC (c) protein expression. Representative confocal images are shown. (e) BV2 cells were treated with LPS (0.5 μgml^{-1}) and JNUTS013 (10 μM) for 12 h, fixed and stained for ASC expression. Representative confocal images are shown. (b), (d), (f) violin plots of NLRP3 and ASC expression level per cell determined by ImageJ from (a), (c) and (e), respectively. Data represent mean, 25th and 75th percentile from n = 50 cells. The whiskers extend to the minimum and maximum values. $^{\#}P < 0.05$ between DMSO and LPS, whereas $^{*}P < 0.05$ between LPS and LPS + JNUTS013 groups by unpaired two-tailed *t*-test in Prism 9.0.

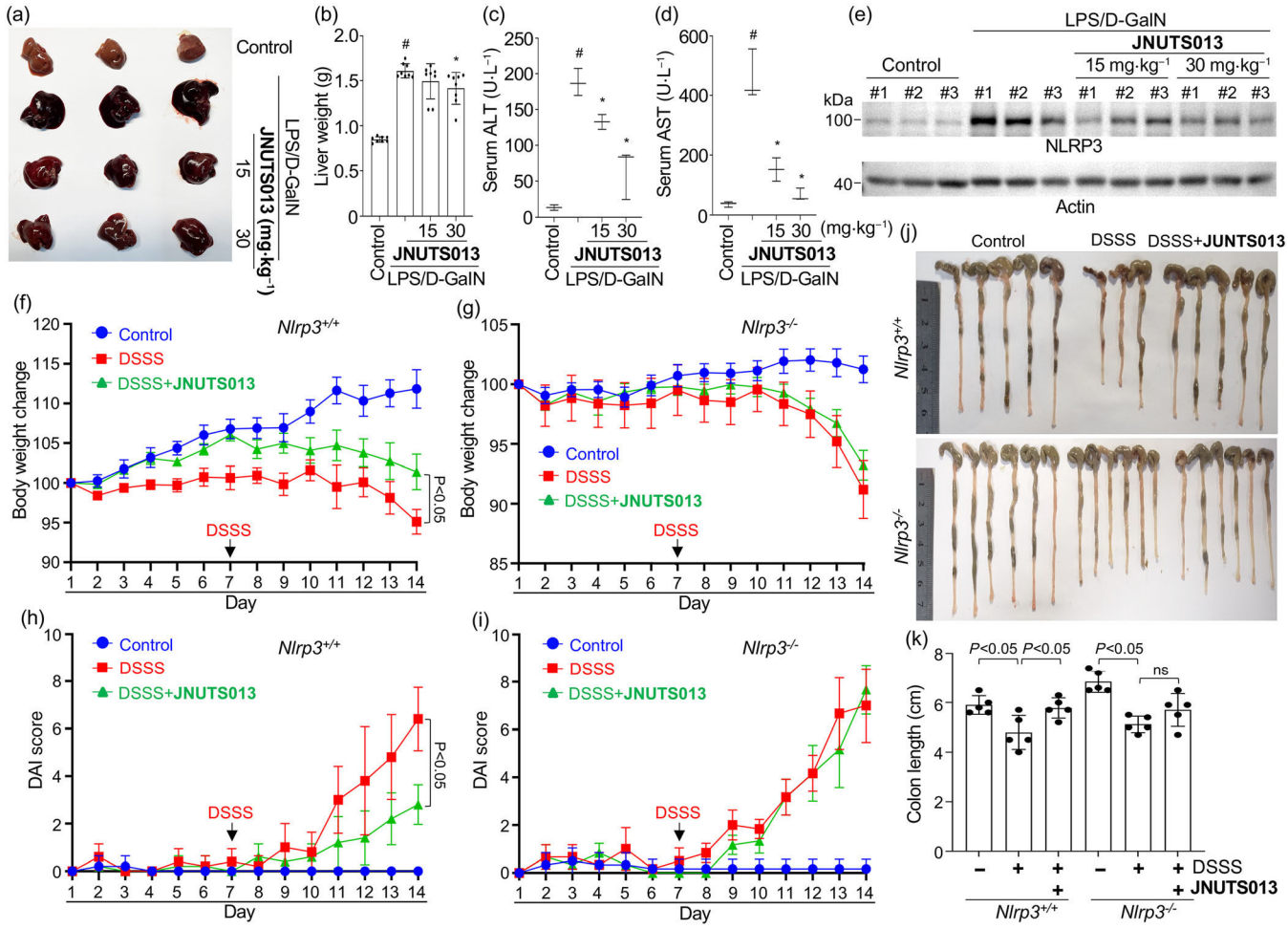

FIGURE 6.

Anti-inflammatory activities of JNUTS013 *in vivo*. Preliminary results showed that intraperitoneal injection of JNUTS013 at or below 30 mgkg^{-1}day^{-1} did not affect the body weight and temperature of mice, and therefore a dose equal or lower than 30 mgkg^{-1} was used. (a) LPS/D-galactomine (D-GalN)-induced acute liver inflammation model. C57 WT female mice were randomly divided into four groups (n = 8 each group): Control, LPS/D-GalN, 15 or 30 mgkg^{-1} JNUTS013 plus LPS/D-GalN and treated as described in Section 2. Representative images of livers are shown. (b) Liver weight in gram. (c, d) Serum levels of ALT and AST enzymatic activities. (e) NLRP3 protein levels in liver tissues from three mice in (a) were assessed. (f, g) Body weight change, (h, i) disease activity index (DAI) score, and (j, k) colon length were measured from DSSS-induced ulcerative colitis in C57 WT and *Nlrp3*$^{-/-}$ mice (n = 5 per group). During experiment, the DSSS group in WT mice had two mice terminated due to illness and two new mice were immediately added to this group, which resulted in tissue collection at different time. Hence, colon images from only three mice were shown for this group in (j); however, the statistical analysis was conducted from a total of five mice. Data are presented as the mean and standard deviation. (b)–(d) and (k): $^{\#}P < 0.05$ compared with the control group and $^{*}P < 0.05$ compared with

the LPS/D-GalN group. (f) and (h): One-way ANOVA with Tukey’s test. ns (not significant). Bar charts were presented when scatter plots did not reveal unusual pattern of the dataset.

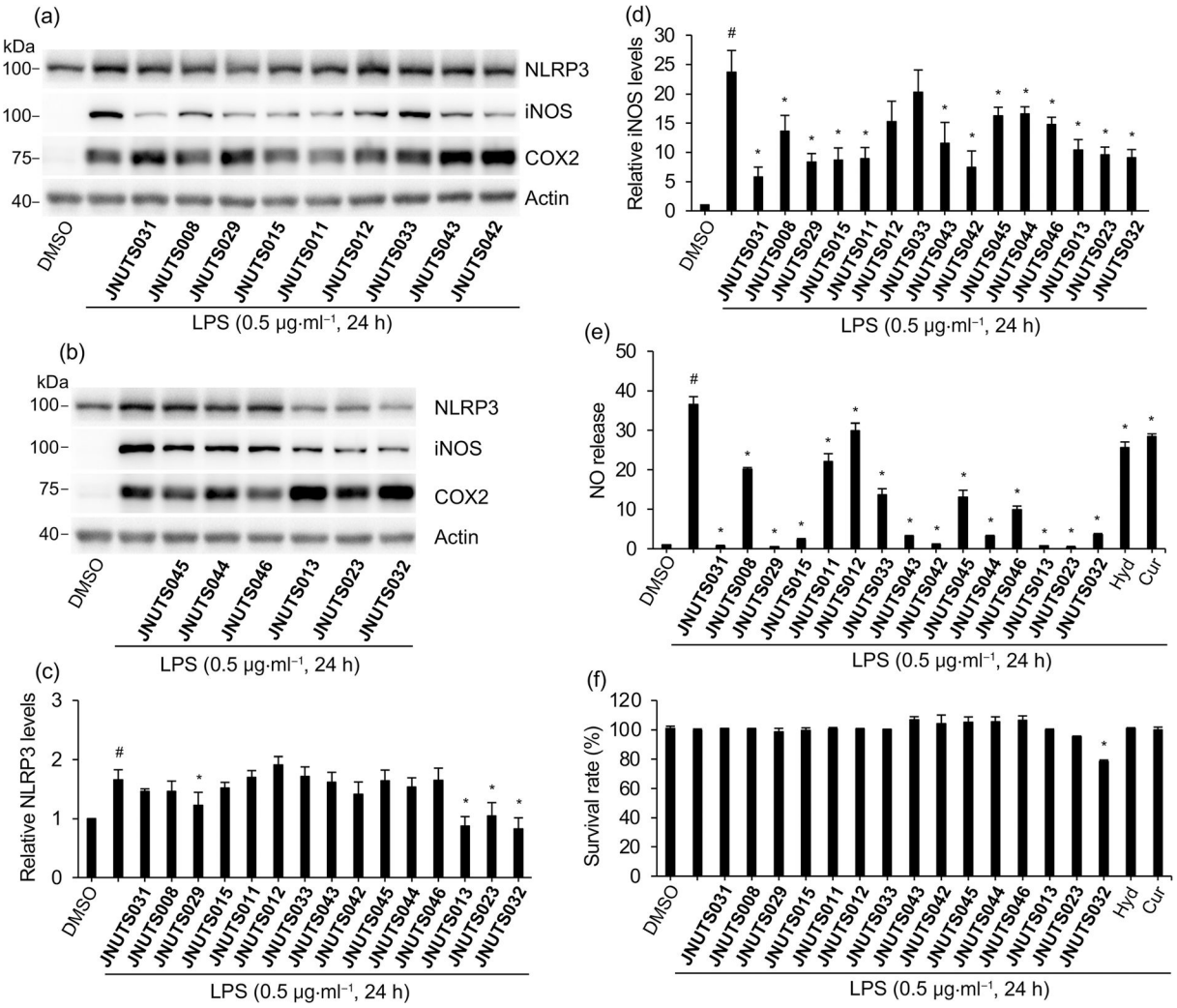

FIGURE 7.

The structure–activity relationship (SAR) of JNUTS013 analogues in inhibiting NLRP3 expression and inflammation. (a, b) RAW264.7 cells were treated with JNUTS013 and analogues at 10 μM for 24 h, and protein expression was examined. (c, d) Quantitation of protein levels of iNOS and NLRP3 from (a) and (b). relative NO release (e) and cell survival rate (f) for RAW264.7 cells being treated with 10 μM JNUTS013 analogues, 20 μM hydrocortisone (Hyd) or curcumin (cur) in the presence of 0.5 μgml^{-1} LPS for 24 h. Data represent mean and standard deviation from five values. $^{\#}P < 0.05$ compared with the DMSO group, whereas $*P < 0.05$ was compared with LPS treatment alone group by non-parametric analysis using prism 9.0. The Y axis represents values of the fold matched control. Bar charts are presented when there were no unusual aspects of data revealed by scatter plots.

TABLE 1

Sequences of qPCR primers.

Primer	Sequence
Nlrp3-F	5′-AGGATCTCGCATTGGTTCTG-3′
Nlrp3-R	5′-GTTGGTTTTGAGCACAGAGG-3′
Pycard-F	5′-TGCTTAGAGACATGGGCTTAC-3′
Pycard-R	5′-CAATGAGTGCTTGCCTGTG-3′
Nos2-F	5′-AGCCTGTGAGACCTTTGATG-3′
Nos2-R	5′-TCAGCCTCATGGTAAACACG-3′
Il-1β-F	5′-TCCTGTGTAATGAAAGACGGC-3′
Il-1β-R	5′-ACTCCACTTTGCTCTTGACTTC-3′
Il-18-F	5′-GTTCACTCTCACTAACTTACATCAAAG-3′
Il-18-R	5′-TCTATAAATCATGCAGCCTCGG-3′
Il-6-F	5′-CAAAGCCAGAGTCCTTCAGAG-3′
Il-6-R	5′-GTCCTTAGCCACTCCTTCTG-3′
Nfkbib-F	5′-GACAGTGACAACAGAGATGAGG-3′
Nfkbib-R	5′-TCAGGAAGAGGTTTGGATGC-3′
Tnfaip3-F	5′-TGTTACTGCCTCTGCGAAAG-3′
Tnfaip3-R	5′-GTCTCTATGCTGGCTTGATCTC-3′
Tnfα-F	5′-TCAATCTGCCCAAGTACTTAGAC-3′
Tnfα-R	5′-CCTGAGCCATAATCCCCTTTC-3′
Ccl2-F	5′-TCCACTACCTTTTCCACAACC-3′
Ccl2-R	5′-GGATCCACACCTTGCATTTAAG-3′
Cxcl10-F	5′-ATCCGGAATCTAAGACCATCAAG-3′
Cxcl10-R	5′-GACCAAGGGCAATTAGGACTAG-3′
Hprt1-F	5′-AGCTTGCTGGTGAAAAGGA-3′
Hprt1-R	5′-CCAAACTCAACTTGAACTCTCATC-3′

TABLE 2

Parameters for calculating the disease activity index (DAI).

DAI scores	Weight loss	Stool consistency	Stool blood
0	0%	Normal	Hemoccult negative
1	1%-5%	Soft but still formed	Hemoccult negative
2	6%-10%	Soft	Hemoccult positive
3	11%-18%	Very soft, wet	Stool blood visible
4	>18%	Diarrhoea	Rectal bleeding